CHAPTER 2

Structural and oxidation-state changes at its non-standard Ni-Fe site during activation of the NAD-reducing hydrogenase from *Ralstonia eutropha* detected by X-ray absorption, EPR, and FTIR spectroscopy

Tanja Burgdorf [a], Simone Löscher [b], Peter Liebisch [b], Eddy Van der Linden [c],
Marcus Galander [d], Friedhelm Lendzian [d], Wolfram Meyer-Klaucke [e],
Simon P. J. Albracht [c], Bärbel Friedrich [a], Holger Dau [b], Michael Haumann [b,]

[a] Humboldt-Universität zu Berlin, Mikrobiologie, Chausseestr. 117, D-10115 Berlin, Germany;
[b] Freie Universität Berlin, Inst. f. Experimentalphysik, Arnimallee 14, D-14195 Berlin, Germany;
[c] University of Amsterdam, Swammerdam Institute for Life Sciences, Biochemistry, Plantage Muidergracht 12, NL-1018 TV Amsterdam, The Netherlands; [d] Technische Universität Berlin, Max-Volmer-Institut für Biophysikalische Chemie und Biochemie, Strasse des 17. Juni 135, D-10623 Berlin, Germany;
[e] DESY, EMBL Outstation, Notkestr. 85, D-22603 Hamburg, Germany.

Keywords

Bioinorganic chemistry, X-ray absorption spectroscopy, EPR, FTIR, Ni-Fe hydrogenase

Abbreviations

DFT, density-functional theory; EPR, electron paramagnetic resonance; EXAFS, extended X-ray absorption fine structure; FTIR, Fourier-transform infrared spectroscopy; Ni, nickel; SH, NAD-reducing soluble hydrogenase; XANES, X-ray absorption near-edge structure; XAS, X-ray absorption spectroscopy

Abstract

Structure and oxidation state of the Ni-Fe cofactor of the NAD-reducing soluble hydrogenase (SH) from *Ralstonia eutropha* were studied employing X-ray absorption spectroscopy (XAS) at the Ni K-edge, EPR and FTIR spectroscopy. The SH comprises a non-standard $(CN)Ni\text{-}Fe(CN)_3(CO)$ site; its hydrogen-cleavage reaction is resistant against inhibition by dioxygen and carbon monoxide. Simulations of the XANES and EXAFS regions of XAS spectra revealed that, in the oxidized SH, the Ni^{II} is 6-coordinated $((CN)O_3S_2)$; only two of the four conserved cysteines, which bind the Ni in standard Ni-Fe hydrogenases, provide thiol ligands to the Ni. Upon the exceptionally rapid reductive activation of the SH by NADH, an oxygen species is detached from the Ni; hydrogen may subsequently bind to the vacant coordination site. Prolonged reducing conditions cause the two thiols that are remote from the Ni in the native SH to become direct Ni ligands, creating a standard-like $Ni^{II}\text{-}X_1S_4$ site (X may be CN, O, or absent), which could be further reduced to form the Ni-C ($Ni^{III}\text{-}H^-$) state. The Ni-C state does not seem to be involved in hydrogen cleavage. Two site-directed mutants (HoxH-I64A, HoxH-L118F) revealed structural changes at their Ni sites and were employed to further dissect the role of the extra CN ligand at the Ni. It is proposed that the predominant coordination by (CN),O ligands stabilizes the Ni^{II} oxidation state throughout the catalytic cycle and is a prerequisite for the rapid activation of the SH in the presence of oxygen.

_____

Introduction

In the course of evolution, nature has convergently invented a variety of enzymes to use the small hydrogen molecule as an energy source (Cammack *et al.* 1997; Berkessel 2001; Horner *et al.* 2002). Hydrogenases are widespread among prokaryotes and are also found in a few unicellular eukaryotes. They can be divided into two major classes: Fe-only hydrogenases are extremely sensitive to oxygen and are mostly found among obligate anaerobes whereas Ni-Fe hydrogenases are also found in aerobic microorganisms (Albracht 1994; Lenz *et al.* 2001; Vignais *et al.* 2001). The Fe-Fe (Peters *et al.* 1998; Nicolet *et al.* 1999) and Ni-Fe (Volbeda *et al.* 1995; Volbeda *et al.* 1996; Higuchi *et al.* 1997; Garcin *et al.* 1999; Frey 2002) cofactors are considered to represent the active sites of hydrogen binding and turnover in hydrogenases (Cammack *et al.* 1997). The Ni-Fe sites in the enzymes that have been crystallized thus far are characterized by a set of common features and these enzymes are therefore called "standard" Ni-Fe hydrogenases (Maroney 1999; Frey 2002). These common features are: (a) The Ni atom is coordinated by the thiol groups of four cysteine residues which are conserved in all amino acid sequences of Ni-Fe hydrogenases (Przybyla *et al.* 1992; Albracht 1994; Vignais *et al.* 2001). Two of the thiols are bridging between the Ni and Fe atoms. (b) The Fe atom carries uncommon ligands, namely two CN and one CO

(Happe *et al.* 1997; Pierik *et al.* 1999). The presence of these diatomic ligands is clearly detectable in FTIR spectra (Bagley *et al.* 1994; Bagley *et al.* 1995; DeLacey *et al.* 1997; Pierik *et al.* 1999; Bernhard *et al.* 2001). (c) Depending on the oxidation state of the enzymes, further ligands (O, H) may be present at the Ni (Albracht 1994; Cammack *et al.* 1997; Higuchi *et al.* 1997; Trofanchuk *et al.* 2000; Foerster *et al.* 2003). (d) In standard Ni-Fe hydrogenases, hydrogen cleavage is inhibited by molecular oxygen; the binding of an oxygen species to the Ni is believed to cause a reversible inactivation of the enzyme (Albracht 1994; Cammack *et al.* 1997).

Despite a wealth of structural and functional information available for Ni-Fe hydrogenases, the mechanism of hydrogen binding and its subsequent heterolytic cleavage at the Ni-Fe cofactor is barely understood (Albracht 1994; Cammack *et al.* 1997; Fontecilla-Camps *et al.* 1997; Frey 2002). DFT calculations (Amara *et al.* 1999; Niu *et al.* 1999; Siegbahn *et al.* 2001; Stein *et al.* 2002) on basis of EPR results suggested the binding of hydrogen species to both the Ni and Fe atoms and changes in the oxidation state of the Ni in the catalytic cycle of hydrogen turnover in standard Ni-Fe hydrogenases.

The facultative chemolithoautotrophic bacterium *Ralstonia eutropha* (for name conventions see Materials and Methods) is capable of using hydrogen as a substrate under aerobic conditions (Friedrich *et al.* 1993; Lenz *et al.* 2002). Consequently, its Ni-Fe hydrogenases are fully functional in the presence of dioxygen (Friedrich *et al.* 1993; Lenz *et al.* 2002), a feature which is unparalleled in the standard hydrogenases. *R. eutropha* harbours three different Ni-Fe hydrogenases. The membrane-bound hydrogenase (MBH) is linked to the respiratory chain (Schink 1979). The so-called regulatory hydrogenase (RH) acts as a hydrogen sensor (Kleihues *et al.* 2000; Bernhard *et al.* 2001). We have recently elucidated the unusual structural features of the Ni-Fe cofactor in the RH during hydrogen sensing (Haumann *et al.* 2003). The cytoplasmic NAD-reducing soluble hydrogenase (SH), which is the subject of the present study, provides reducing equivalents mainly for CO_2 fixation.(Schneider *et al.* 1976) The SH has extensive similarity to NADH-ubiquinone oxidoreductases (Complex I) (Pilkington *et al.* 1991; Albracht *et al.* 2000).

The SH consists of a heterotetramer (Schneider *et al.* 1976). This tetramer is composed of two different functional modules, namely a NADH-dehydrogenase (or –diaphorase) dimer and a hydrogenase dimer (Erkens *et al.* 1996; Massanz *et al.* 1998). HoxH, the large subunit of the hydrogenase part contains the four conserved cysteine residues, which, in standard Ni-Fe hydrogenases, provide thiol ligands to the Ni-Fe cofactor. The HoxY protein is a truncated version of the small subunit of standard hydrogenases and presumably harbours only the proximal [4Fe-4S] cluster. The small diaphorase subunit HoxU likely accommodates at least one [4Fe-4S] cluster and one [2Fe-2S] cluster. The large subunit HoxF contains one [4Fe-4S] cluster, one FMN cofactor (here termed FMN-b) and provides the NAD binding site (Tran-Betcke *et al.*

1990). Recently a second FMN, called FMN-a, was identified in the SH (Van der Linden *et al.* 2004a). Both dimers mediate the reduction of artificial electron acceptors at the expense of H_2 or NADH, respectively. The reduction of NAD^+ by H_2, however, requires the tetrameric enzyme (Massanz *et al.* 1998; Massanz *et al.* 1999; Burgdorf *et al.* 2002). The electrons derived from H_2 cleavage are presumably transferred from the Ni-Fe site via FMN-a, the [4Fe-4S] and [2Fe-2S] clusters to the FMN-b and subsequently to NAD^+ (Erkens *et al.* 1996; Van der Linden *et al.* 2004a).

Biochemical and spectroscopic investigations have revealed several unusual features of the SH. (i) The SH is fully active in the presence of O_2 and also not inhibited by CO (Schneider *et al.* 1976; Happe *et al.* 2000). (ii) In its "as isolated", oxidized state the SH is EPR-silent. EPR signals due to Ni^{III} which are characteristic for the inactive states, denoted as Ni-A and Ni-B in standard hydrogenases (for an overview see ref. (Cammack *et al.* 1997)), are not found in the SH (Schneider *et al.* 1979; Erkens *et al.* 1996; Schneider *et al.* 1996; Happe *et al.* 2000). (iii) Standard hydrogenases are activated by incubation with H_2 for minutes (ˋreadyˊ enzyme) or several hours (ˋunreadyˊ state) (George *et al.* 2004; Kurkin *et al.* 2004). The SH is only slowly activated with H_2 alone (45 min at 30 ℃) (Schneider *et al.* 1976). Rapid activation is achieved (within a few seconds) after the addition of catalytic amounts of NADH (Happe *et al.* 2000) (iv) The Ni in the SH is usually EPR-silent under a variety of redox conditions, suggesting a Ni^{II} oxidation state (Schneider *et al.* 1976; Schneider *et al.* 1979; Erkens *et al.* 1996). However, after prolonged reduction (Erkens *et al.* 1996; Müller *et al.* 1997) a Ni-C signal has been observed. Whether the Ni-C state is an intermediate in the catalytic cycle of the SH is under debate (Müller *et al.* 1997; Happe *et al.* 2000; Van der Linden *et al.* 2004b) In standard hydrogenases the Ni-C signal was attributed to a $Ni^{III}-H^-$ state (Cammack *et al.* 1997; Brecht *et al.* 2003; Foerster *et al.* 2003) (v) FTIR analysis suggested the presence of two additional CN molecules in the SH, one is bound to the Fe and one to the Ni, resulting in a [(CN)Ni-Fe(CN)₃(CO)] active site (Happe *et al.* 2000; Van der Linden *et al.* 2004a). The presence of four cyanide groups has now been confirmed by chemical analysis; upon specific removal of the CN bound to the Ni, the enzyme becomes sensitive to oxygen (Van der Linden *et al.* 2004b). So far, the atomic structure of the Ni-Fe cofactor is unknown as crystals of the SH are not yet available. The relations between the unusual structural and spectroscopic properties and the catalytic function are widely unclear.

This study focuses on the unravelling of the structure and function of the Ni-Fe site of the SH by using X-ray absorption spectroscopy (XAS) at the Ni K-edge, EPR, and FTIR spectroscopic techniques. For the first time, complementary simulations of the XANES and EXAFS regions of XAS spectra were employed to deduce the atomic structure of the Ni site. To obtain new insights into structure-functional relations, changes at the Ni-Fe cofactor of the SH were investigated under a variety of redox

conditions. Furthermore, we compared the structural features of the Ni-Fe site in two mutants with altered catalytic properties.(Massanz *et al.* 1999; Burgdorf *et al.* 2002) One (I64A) was inactive in H_2 cleavage whereas the other one (L118F) showed oxygen-sensitive catalytic activity.

The following questions were specifically addressed: **(1)** What are the structural features of the Ni-Fe cofactor in the native SH in its "as-isolated" state? **(2)** Which structural changes are induced by the reactions with the substrates? **(3)** Does the oxidation state of the Ni change during the catalytic cycle? **(4)** How are the structural features of the Ni-Fe site related to the unusual properties of activation and catalysis of the SH?

Materials and Methods

Bacterial strains and growth conditions

Ralstonia eutropha H16 (Yabuuchi *et al.* 1995) was originally isolated as *Hydrogenomonas eutropha* H16 (Wilde 1962), then renamed *Alcaligenes eutrophus* (Davis *et al.* 1969), and very recently again renamed *Wautersia eutropha* (Vanechoutte *et al.* 2004). In this manuscript we decided to use the established name R. eutropha for consistency with our previous work on the SH (Happe *et al.* 2000; Van der Linden *et al.* 2004a; Van der Linden *et al.* 2004b).

The strains and plasmids used in this study are listed in Table 1. R. eutropha was cultivated in mineral salts medium containing 0.4 % (w/v) fructose or a mixture of 0.2 % (w/v) fructose and 0.2 % (v/v) glycerol (FGN medium).(Friedrich *et al.* 1981) Under standard conditions the medium was supplemented with 1 µM $NiCl_2$. Large scale cultivation was performed in 10 and 50 l fermenters (Braun Biotech). Wild type SH was isolated from both H16 and HF359. For cultivation of SH mutants plasmids pGE475 and pGE482 (Table 1) were transferred into the hydrogenase-negative strain HF424.

Table 1. Plasmids and Plasmids

	relevant characteristics	source or reference
Ralstonia eutropha strains		
H16	SH^+MBH^+	DSM 428, ATCC 17699
HF359	MBH^-	(Bernhard *et al.* 1996)
HF424	SH^-MBH^-	(Massanz *et al.* 1998)
Plasmid		
pGE475	HoxH[I64A]	(Burgdorf *et al.* 2002)
pGE482	HoxH[L118F]	(Burgdorf *et al.* 2002)

Protein purification

For SH purification cells from a 10 l fermenter (50-60 g) were resuspended in 40 mL 50 mM potassium phosphate buffer (pH 7.0) containing 0.1 mM PMSF and DNaseI and passed twice through a chilled French Press cell at 1100 psi. After ultracentrifugation at 100.000 x g the SH was purified in a four-step procedure adapted from refs. (Friedrich *et al.* 1982; Schneider *et al.* 1996) Ammonium sulfate was added in two steps to 30 and 60 % saturation. The pellet was redissolved in an appropriate volume of 50 mM potassium phosphate buffer (pH 7.0). After dialysis against fresh buffer the protein solution was applied to a DEAE Sephacel column (Pharmacia) and eluted with a linear gradient of 0 to 350 mM KCl in 50 mM potassium phosphate buffer (pH 7.0). SH-containing fractions were combined and concentrated by ultrafiltration up to 10-20 mg protein/mL (100 kDa membrane; Amicon). If necessary the combined fractions after DEAE were precipitated by 60 % ammonium sulphate and were further purified by hydrophobic interaction on a phenylsepharose column (Pharmacia). The pellet was redissolved in an appropriate volume of 200 mM potassium phosphate buffer (pH 7.0) and applied to the column. After washing with 200 mM and 50 mM potassium phosphate buffer (pH 7.0) (one column volume each), the SH was eluted using a linear gradient from 10 mM potassium phosphate buffer to water. The appropriate fractions were combined, dialysed against 20 mM Tris-HCl buffer (pH 8.0), concentrated and stored in liquid nitrogen. For XAS studies all samples were further purified by gelfiltration on a Superdex 200 column (Pharmacia) in 20 mM Tris-HCl buffer (pH 8.0). SH-containing fractions were pooled and further concentrated by ultafiltration up to final concentrations of ca. 150 mg/mL. The purity of the samples was verified by SDS-gel electrophoresis. Protein concentrations were determined by the method of Bradford(Bradford 1976) using bovine serum albumin as a standard.

Enzymatic characterization of SH sample

Hydrogenase activity ($H_2 \rightarrow NAD$ electron transfer) was assayed by measuring spectrophotometrically the H_2-dependent reduction of NAD (1 mM final concentration) at 340 nm in 50 mM H_2-saturated Tris-HCl buffer (pH 8). H_2 and NADH oxidation with the artificial electron acceptor benzyl viologen (BV; 3 mM final concentration) was determined at 578 nm. NADH oxidation (final concentration 1 mM) was measured in N_2-saturated buffer. H_2 production from NADH (1 mM final concentration) was measured amperometrically at 30 °C with a Clark-type electrode in 50 mM potassium phosphate buffer (pH 6.0). The specific activities of the purified SH samples subjected to XAS analysis, are summarized in Table 2.

Table 2.   Specific Activities of Purified SH Preparations
Determined under Anaerobic Conditions as Outlined in Ref49

SH sample	Specific enzymatic activity in U/mg			
	H_2-NAD$^+$	H_2-BV	NADH-BV	NADH-H_2
Wild type SH	61	25	30	0.6
HoxH[I64A]-modified SH	0	0.2	47	n.d.[1)]
HoxH[L118F]-modified SH	4	1.2	37	n.d.
"Inactive" wild type SH	9.2[2)]	1.0	20	0.1

[a] n.d., non detectable. [B] For further details, see Materials and Methods section

The best wild type SH preparations obtained in our hands exhibited a specific activity of 61 U/mg. Such high activities could only be determined in samples taken from enzyme solutions with a protein concentration up to 60 mg/mL. With samples taken from enzyme at higher protein concentrations the activity decreased down to 60 %. Concentrating the SH above 100 mg/mL resulted in protein solutions that contained high molecular weight aggregates (as detected during gel filtration). The formation of aggregates could not be prevented by the addition of 5 % (w/v) glycerol to the sample buffer. Up to 25 % of activity could be regained by incubating the enzyme under diluting conditions. Not only the H_2-NAD activity decreased upon concentration but also the H_2-BV and the NADH-BV activities. The latter activity does not depend on an intact Ni-Fe active site. These results indicate that the NADH and BV binding sites are less accessible in very concentrated SH samples and that the moderate loss of H_2-NAD activity in these samples is not caused by alterations at the Ni-Fe site itself.

Determination of the Ni and Fe contents of several concentrated SH samples by atomic absorption spectroscopy (AAS, performed in the laboratory of Dr. K. Irrgang, Technical University Berlin) yielded 0.55 Ni and 9.62 Fe per SH protein on the average (the error in the AAS measurements is less than 10 % of the determined values). These values seemingly can not be taken at face value as the Bradford method (Bradford 1976) of protein determination may overestimate the SH content by up to a factor of 1.5 (Albracht *et al.* 2003; Van der Linden *et al.* 2004a). When this overestimation is taken into account the enzyme contains about 0.83 Ni and 14.4 Fe atoms. This is close to the expected values of 1 Ni and 15 Fe (see Introduction). The specific activities given in this study represent the uncorrected values. (We note that a higher protein overestimation (up to a factor of two) may yield values of up to 1.10 Ni and 19.24 Fe per SH. Whereas the Ni per SH ratio remains close to one, the higher Fe content would allow for an additional [4Fe4S] cluster. Indeed, indications from sequence comparison

for a possible additional Fe-S binding motif in the HoxU subunit of the SH have been obtained.[107] In any event, the conclusions on the structure of the Ni site of the SH derived later in this manuscript are not affected by the presence of such an additional Fe-S cluster.)

SH samples from wild type *R. eutropha* with a specific H_2-NAD activity of ≤10 U/mg were called "inactive". The low SH activity in the soluble extracts was unstable, i.e. up to 85 % of the activity was lost upon storage on ice for 28 hours. The stability of the SH in soluble extracts was dependent on protein concentration and growth conditions. Extracts with concentrations above 60 mg/mL seemed to be less stable. Moreover cells grown in 50 l scale resulted mostly in less active SH than cells cultivated in a 10 l fermenter. The H_2-oxidizing activity of inactive SH samples was more strongly affected than the diaphorase (NADH-BV) activity (Table 2). The L118F mutant was isolated under aerobic conditions. Activity in the soluble extract rapidly decreased and purified protein exhibited low H_2-NAD activity (Table 2), which turned out to be O_2-sensitive (see below).

Analysis of oxygen sensitivity

To determine the oxygen sensitivity, the H_2-oxidizing activity with NAD or MV was measured as in ref. (Van der Linden *et al.* 2004b) under aerobic and anaerobic conditions at 30 °C in a 2.1 mL cell with a Clark electrode (type YSI 5331) for polarographic measurement of H_2 (Coremans *et al.* 1992b). For routine H_2-consumption measurements under aerobic conditions the cell was filled with aerobic buffer (50 mM Tris-HCl, pH 8.0), 5-10 µL enzyme and H_2-saturated water to a final H_2 concentration of 36 µM. Then, NADH (5 µM) was added to activate the enzyme, followed by either benzyl viologen (BV, 2.5 mM) or NAD^+ (5.0 mM) as the electron acceptor. When anaerobic conditions were used, all solutions were flushed with Ar before use and glucose (50 mM) plus glucose oxidase (9 U/ml) were added to the reaction medium 3 min before the NADH addition. This minimized interference of oxygen. NADH oxidation with $K_3Fe(CN)_6$ as electron acceptor was measured aerobically in 50 mM Tris-HCl buffer (pH 8.0) at 30 °C monitoring the absorption decrease at 420 nm using a Zeiss M4 QIII spectrophotometer ($\varepsilon = 1$ mM^{-1}cm^{-1} for $K_3Fe(CN)_6$). An enzyme sample (5 µl) and NADH (1.25 mM) were added and 3 min later the reaction was started by the addition of $K_3Fe(CN)_6$ (1 mM). Before use, H_2 was passed over a palladium catalyst (Degussa, Hanau, Germany; type E236P), and Ar was passed through an Oxisorb cartridge (Messer-Griesheim, Düsseldorf, Germany), to remove residual O_2.

Under anaerobic conditions the wild type SH exhibited an H_2-NAD activity of 61 U/mg and an H_2-MV activity of 40 U/mg. Under aerobic conditions both activities were 20 % lower. For the L118F mutant 4 U/mg (H_2-NAD) and 1.2 U/mg (H_2-MV)

were detected under anaerobic conditions. Under aerobic conditions both activities were in the same range but the H_2-MV activity ceased within 10 seconds whereas it remained stable for several minutes in the absence of oxygen. The wild type SH did not show an inhibition by dioxygen under those conditions; both activities were stable for several minutes in the presence and absence of oxygen.

Reductive treatments and XAS sample preparation

Before reductive treatment, concentrated protein samples were degassed several times under nitrogen. For reductive treatments in the presence of hydrogen, the atmosphere was exchanged by repeated degassing. Reductant stock solutions were freshly prepared (NADH, NADH+NAD, Na-dithionite, or dithiothreitol (DTT)) in 100 mM Tris-HCl buffer (pH 8), 100 mM MES (pH 6). All solutions were bubbled with nitrogen for 15 minutes. Samples finally contained concentrations of 10 mM NADH, 10 mM of mixtures of NADH and NAD, 10 mM dithionite, or 1 mM DTT, and protein concentrations between 0.7 and 1.2 mM. After reductants were added, the samples were incubated at room temperature for 10 min (dithionite, DTT) or 3 min (NADH / NAD). For complete activation, samples containing 25 µM NADH were prepared and stored under hydrogen for 12 h on ice. After incubation, samples were filled under argon or hydrogen atmosphere into specialized sample holders with 12 µm thick Kapton windows (ca. 20 µl protein solution per sample holder) and immediately frozen in liquid nitrogen. The same samples were used for both XAS and EPR measurements; EPR measurements were carried out before and after XAS measurements. Aliquots of samples were separately frozen for FTIR measurements.

X-ray absorption spectroscopy

X-ray absorption spectra at the nickel K-edge were collected at beamline D2 of the EMBL Hamburg outstation (HASYLAB, DESY, Hamburg, Germany) during three runs. Fluorescence-detected XAS spectra were measured at 20 K (Iuzzolino *et al.* 1998; Schiller *et al.* 1998; Haumann *et al.* 2003) (monochromator detuning to 70 % of maximum intensity; scan range: 8150 – 9100 eV). An absolute energy calibration was performed by monitoring the Bragg reflections of a crystal positioned at the end of the beamline (Pettifer *et al.* 1985). For each element of the 13-element solid-state germanium detector, the total count-rate was kept well below 30000 s^{-1}; the output signal was corrected for detector saturation. The spot size of the X-ray beam on the sample was 4.5 x 1.2 mm; not more than 3 scans of ~60 min duration were taken on the same spot of the sample. Comparison of the first and third scan revealed no evidence for

radiation damage to the samples as the Ni K-edge shape and energy remained unchanged. EXAFS spectra represent the average of 6-12 scans.

XAS-spectra were averaged after energy calibration of each individual scan, normalized, and EXAFS oscillations were extracted as previously described (Dau *et al.* 2003). The energy scale of Ni EXAFS spectra was converted to *k*-scale using E_0 = 8333 eV (Gu *et al.* 1996; Haumann *et al.* 2003); E_0 was allowed to vary by ±2 eV during EXAFS simulations. Unfiltered k^3-weighted spectra were used for least-squares curve-fitting (with the in-house software SimX (Dittmer 1999)) and for calculation of Fourier-transforms (FTs). The shown FTs represent *k*-values ranging from 1.98 to 12.85 $\mathring{A}^{-1}$ (15-630 eV above E_0). Data was multiplied by a fractional cosine window (5 % at low and high *k*-side). For EXAFS simulation, complex backscattering amplitudes were calculated using FEFF 7 (Zabinsky *et al.* 1995): the value of S_0^2, the amplitude reduction factor, was 0.9, which facilitated the correct determination of the coordination number of six from the EXAFS spectrum of the $[Ni(H_2O)_6]^{2+}$ complex (see ref. (Haumann *et al.* 2003)). The given 'K-edge energies' refer to 50 % of the normalized absorption at the Ni K-edge.

Multiple-scattering calculation

XANES simulations were performed on a personal computer using the *ab-initio* code FEFF 8.2 (Ankudinov *et al.* 1998) with both the full-multiple-scattering (FMS) and the self-consistent-field (SCF) options activated. The same potential was used for atoms of each species where the Ni-atom distance deviated by not more than 0.1 $\mathring{A}$; for longer distances individual potentials were used. Further technical details: muffin-tin overlap of 15 %; l_{max} = 3; energy-dependent part of the exchange-correlation potential calculated by Hedin-Lundqvist model / atomic background by von-Barth-Hedin model, no imaginary part added; S_0^2 set to unity; correlated Debye model (T_{Debye} = 410 K and measurement temperature of 20 K). Calculated XANES spectra were shifted by 1.5 eV to lower energies and an offset of 1 % of normalized fluorescence was subtracted to allow for better comparison with the experimental spectra. No further attempts have been made to optimize the matching between experimental and calculated spectra. Atomic coordinates for FEFF input files of XANES calculations were generated using the program Hyperchem 6 (Hypercube) and Ni-ligand distances derived from EXAFS simulations or from the literature (for further details see Results section). When capping hydrogens or methyl groups (see Fig. 2) were introduced into the structures, the positions of these atoms were optimized (employing fixed Ni-ligand distances) using the standard routines of the Hyperchem program.

ERP spectroscopy

EPR spectroscopy was performed on a Bruker ESP 300E spectrometer equipped with a helium cryostat (Oxford) using a microwave frequency of 9.57 GHz, a modulation frequency of 10 kHz, and a modulation amplitude of 1 mT. For further conditions see figure captions. EPR signals were checked for the absence of saturation by comparative measurements at 0.25 and 1 mW of microwave power.

FTIR measurements

FTIR spectroscopy was carried out on a BioRad FTS60A spectrometer equipped with a MCT detector as previously described (Pierik *et al.* 1999). FTIR spectra were baseline corrected using the BioRad software available with the spectrometer.

Results

The structural features of the Ni site in the oxidized SH

Analysis of the XANES and EXAFS regions of an XAS spectrum provides information on the atomic structure and on electronic properties of the nickel site. In the XANES region (K-edge), the area of the pre-edge peak (dipole-forbidden $1s{\rightarrow}3d$ transitions) is related to the Ni coordination-number and –geometry, the sharpness and maximal magnitude of the edge depend on the chemical nature of the primary Ni ligands and on the site geometry, and the position of the K-edge on the energy scale may be indicative of the oxidation state of Ni (Colpas *et al.* 1991; Rehr *et al.* 2001; Dau *et al.* 2003; Haumann *et al.* 2003). The EXAFS region, on the other hand, contains information on the number and chemical identity of ligands and on the Ni-ligand distances up to about 4 Å (Teo 1986; Stöhr 1992; Koningsberger *et al.* 2000; Scott 2000; Dau *et al.* 2003).

Table 3.   Ni k-edge (XANES) Characteristics of the Wild-Type (WT)
And I64A and L1118F Mutant SH Samples

sample	K-edge maximum[a] (±0.02)	K-edge energy[b], -8300 eV (±0.05 eV)	Ni coordination[f]
WT oxidized	1.53	41.31	$C_1O_3S_2$
WT +NADH	1.43	41.16	$C_1O_2S_2$
WT +NADH+H_2	1.47	41.18	$H_1C_1O_2S_2$
WT +dithionite	1.10	39.17	$(H,O)S_4$
WT inactive	1.25 (1.14)[c]	39.56 (39.28)[c]	$(O_1)S_4$
I64A all conditions	1.66	41.64	O_4S_2
L118F oxidized	1.29	40.77	$C_1O_2S_3$
L118F +NADH	1.21	40.50	$C_1O_1S_3$
L118F +NADH+H_2	1.30	40.65	$H_1C_1O_1S_3$
D. gigas ox. / red.[d]	1.09 / 1.06	40.40 / 39.20	O_1S_4 / S_4
$[Ni(H_2O)_6]^{2+}$ [e]	1.84	42.07	O_6

[a]The K-edge maximum refers to the normalized fluorescence intensity at 8348 eV; [b]The K-edge energy was determined at 50 % of normalized fluorescence; [c]Values in parenthesis are for the XANES spectrum resulting after subtraction of 16 % of the spectrum of the oxidized native SH; [d]Values for the *D. gigas* hydrogenase have been taken from refs. (Gu *et al.* 1996; Gu *et al.* 2003), in the oxidized state (ox.) Ni[III] and in the reduced state (red.) Ni[II] is present; [e] For EXAFS parameters of $[Ni(H_2O)_6]^{2+}$ see ref. (Haumann *et al.* 2003); [f]For the respective EXAFS fit parameters see Table 5.

Figure 1A (black line) shows the XANES spectrum at the Ni K-edge of the as-isolated, air-oxidized SH. The spectrum is similar to previously reported ones (Gu *et al.* 1996; Müller *et al.* 1997; Bleijlevens 2002). The small pre-edge peak (marked by an arrow) is similar to the one of the $[Ni(H_2O)_6]^{2+}$ complex (Fig. 1A, lower inset), strongly suggesting a six-coordinated Ni with near octahedral geometry. The sharpness of the K-edge and its maximal magnitude (μ(8348 eV) = 1.53, Table 3) is much larger than in any other Ni-Fe hydrogenase investigated so far. Edge magnitudes exceeding 1.4 have only been observed in Ni model compounds with 6-coordinated Ni and in the presence of ≥4 O,N ligands (Eidsness *et al.* 1988; Colpas *et al.* 1991; Haumann *et al.* 2003). Thus, in the SH, the Ni is likely not bound by four "soft" sulphur ligands as in standard hydrogenases, but its ligation is dominated by "hard" O, N, and C ligands.
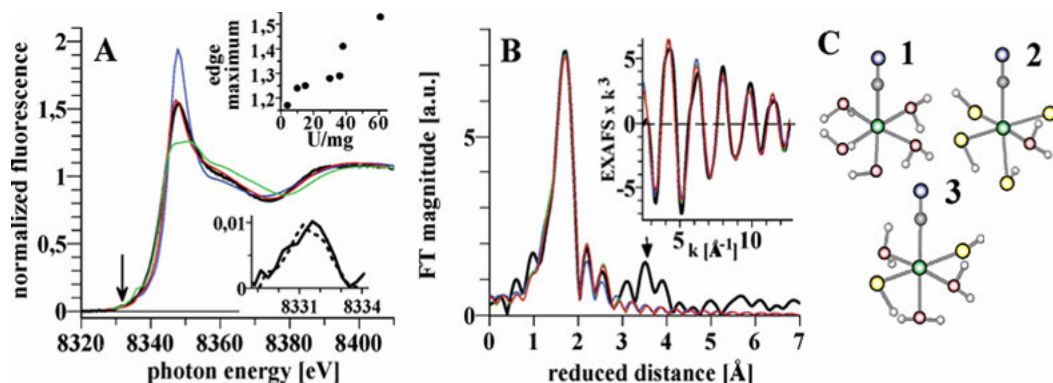
Figure 1. XAS spectrum of the oxidized SH: XANES and EXAFS simulations. (A) XANES spectrum of the oxidized SH (black) and simulations (colored) using the Ni-ligand distances of the respective EXAFS fit approaches (Table 4). The lower inset compares the pre-edge peaks (arrow in the main trace) of the oxidized SH (solid line) and the [Ni(H2O)6]2+ complex (dotted line). The pre-edge peaks have been baseline corrected by subtraction of a spline through the respective K-edges. The upper inset shows the K-edge maximum at 8348 eV as a function of the anaerobic H2-NAD activity (U/mg) for various SH preparations. (B) Fourier transform of the experimental EXAFS spectrum (black) and simulated spectra according to fit approaches I (blue), II (green), and VI (red) listed in Table 4. The inset shows a backtransform (black) of the experimental FT using a window from 0 to 5 Å of reduced distance. (The backtransform has solely been calculated to generate a noise-free spectrum for better comparison with simulation results. It was not involved in the simulation itself.) The colored lines in the inset represent the respective fit approaches also shown in the main trace. (C) The atomic structures underlying the XANES simulations. (1) Ni-C1O5, (2) Ni-O2S4, (3) Ni-C1O3S2 (Ni, green; S, yellow; O, red; N, blue; C, gray; H, white); for the respective Ni-ligand distances, see Table 4 (fits I, II, VI).

The largest maximum (1.53) of the K-edge was observed in an SH sample which showed the highest specific activity (61 U/mg, Table 2 and Fig. 1A). In fact, the maximum of the K-edge is strongly correlated to the specific activity. Smaller maxima were obtained with samples having a lower activity, i.e. the maximal value was only 1.19 in a sample showing an activity of only 9 U/mg (Fig. 1A, upper inset). Noteworthily, the K-edge magnitude in the as-isolated state was similar in the presence of ferricyanide added as an additional oxidant (data not shown). To check whether Ni might be released from the SH to the bulk (as a hexaquo $[Ni(H_2O)_6]^{2+}$ complex, see Fig. 2A), thereby increasing the maximum of the Ni K-edge, SH samples were thawed after X-ray irradiation for ~4 h, exposed to oxygen at room temperature for several minutes, and refrozen. Even after this relatively harsh treatment, the K-edge maximum was virtually unchanged (data not shown), suggesting the absence of Ni release from the SH. AAS measurements revealed the presence of near-stoichiometric amounts of Ni

per SH protein (see Materials and Methods). The contamination of SH samples with unbound Ni is therefore estimated to be small, presumably less than 10 %.

We conclude: **(i)** The Ni in the investigated samples is firmly bound to the SH. EPR data (see below) and the above XAS measurements reveal that the population of the oxidized state in the as-isolated SH sample is close to 100 %. **(ii)** The exceptionally large maximum of the Ni K-edge is a feature of the Ni site in the native oxidized SH.

Figure 1B shows the Fourier-transform (FT) of the EXAFS oscillations (inset) of the oxidized SH (black lines). The main FT peak is located at a reduced distance of ~1.8 Å (the true Ni-ligand distances are by ~0.4 Å larger than the reduced distances of Fourier-transformed spectra); smaller peaks well above the noise level are discernable in the region of 3-4 Å (arrow in Fig. 1B).

As pointed out above, the XANES of the oxidized SH suggests a six-coordinated Ni with clear emphasis on O, N (or C) ligands. Since O and N ligands can hardly be distinguished by EXAFS analysis because of their similar backscattering magnitudes we will discuss only the presence of oxygen ligands as no indication for Ni ligation by nitrogen has, so far, been obtained in any hydrogenase. By varying the O to S ratio in simulations of EXAFS oscillations we tried to clue on the precise number of S-ligands to the Ni in the SH.

In Table 4-I, the EXAFS spectrum was simulated assuming a (CN) O_5-coordination of the Ni; an unlikely alternative since there are four conserved cysteine residues in the amino acid sequence of the HoxH subunit of the SH (Erkens *et al.* 1996). However, this approach yields a reasonable EXAFS fit (Fig. 1B, blue lines).

Recent crystallographic and XAS investigations on the Ni-Fe hydrogenase of *D. gigas* revealed that the distance to the Ni of terminal sulphurs is significantly shorter than to those that bridge between Ni and Fe (Gu *et al.* 2003). A Ni site comprising 2 S-shells with different Ni-S distances and two S-ligands each and, in addition, one O and one (CN) ligand also yielded reasonable fit parameters (Table 4-II; Fig. 1B, green lines). The EXAFS oscillations of the long and short Ni-S vectors mostly interfere destructively since they are almost counterphasic in the *k*-space (data not shown). Thus the presence of four such vectors can not be deduced from EXAFS simulations without independent further structural information.

A simulation assuming 2 S and 4 O ligands immediately yielded a good fit (Table 4-III). Invoking also a Ni-Fe vector slightly improved the result (fit IV), however, the Debye-Waller parameter of the S-shell remained unreasonably large. Using two S-shells with ~0.2 Å different Ni-S distance now provided reasonable Debye-Waller parameters (ref. (Eidsness *et al.* 1988) and references therein) for both shells (fit V). Including a C-atom from the CN ligand yielded an extraordinarily small R_F-value of only ~6 % (fit VI, Fig. 1A, red line).

Table 4.   Parameters of alternative fit approaches of the EXAFS spectrum of the oxidized SH[a].

fit approach	shell	N_i [per Ni]	R_i [Å]	σ_i^2 [10^{-3} Å^2]	R_F [%]
I	C	1.0	1.95	1.5	7.9
	O	5.0	2.06	4.9	
II	C	1.0	1.98	1.0	7.6
	O	1.0	2.02	2.3	
	S	2.0	2.23	2.4	
	S	2.0	2.41	5.1	
	Fe	1.0	2.86	11.2	
III	O	4.0	2.06	4.5	9.3
	S	2.0	2.35	32.4	
IV	O	4.0	2.06	4.5	8.6
	S	2.0	2.35	35.7	
	Fe	1.0	2.90	14.4	
V	O	4.0	2.04	7.8	6.9
	S	1.0	2.24	1.6	
	S	1.0	2.42	4.8	
	Fe	1.0	2.88	12.9	
VI	C	1.0	1.98	1.3	6.3
	O	3.0	2.05	7.0	
	S	1.0	2.24	1.5	
	S	1.0	2.43	5.6	
	Fe	1.0	2.88	13.0	

[a]N_i, coordination number per absorbing Ni atom of the individual backscatterer shells; R_i, absorber-backscatterer distance; σ_i^2, EXAFS Debye-Waller parameter; R_F, weighted error factor defined as in ref.(Meinke *et al.* 2000). The C-atom in the simulations belongs to the CN ligand at the Ni.

The determined Ni-Fe distances (Table 4) from EXAFS simulations are tentative as the Ni-Fe vector apparently only weakly contributes to the EXAFS (see above and also sections below). However, inclusion or exclusion of such a vector in the simulations only marginally altered the EXAFS fit results for the first sphere ligands. Furthermore, a Ni-Fe vector can seemingly be neglected in XANES simulations (see next section). Thus, we consider the derived distances between Ni and its first sphere ligands as reliable.

The EXAFS simulation curves calculated on basis of the chemically clearly distinct fit approaches I, II, and VI are almost indistinguishable (Fig. 1B). Seemingly, the structure of the Ni site and the number of S-ligands to the Ni can not unambiguously be deduced from EXAFS simulations (see also refs. (Gu *et al.* 1996; Davidson *et al.* 2000; Gu *et al.* 2003; Haumann *et al.* 2003)). (To improve the situation, in ref. (Gu *et al.* 2003) EXAFS spectra were measured up to higher energies where oscillations from

heavier atoms (e.g. the Fe, long-distance S) are expected to be dominant. Problematic is the subtraction of the Cu K-edge (at ~8979 eV) from Cu contaminations (Gu *et al.* 2003) and the at least three-fold increase in the measuring time for a reasonable signal-to-noise ratio at *k*-values up to ~16.) A promising new approach to obtain additional structural information is the quantitative analysis of the XANES region of the XAS spectrum.

Simulation of the XANES region of XAS spectra

Due to recent progress in XAS theory and its implementation in modern full-multiple-scattering code (Ankudinov *et al.* 1998) ab-initio calculations of the K-edge have become feasible (for recent examples see refs. (Rehr *et al.* 2001; Benfatto *et al.* 2003; Dau *et al.* 2003; Haumann *et al.* 2003; Mijovilovich *et al.* 2003)). To judge the quality of K-edge simulations, we first calculated the XANES spectrum of a simple compound (see insets in Fig. 2) with pure O-ligation, the $[Ni(H_2O)_6]^{2+}$ complex, and of a much more complex structure with mixed O,S-ligation, the Ni-Fe site of the crystallized *D. gigas* hydrogenase (Volbeda *et al.* 1995). The respective Ni-ligand distances were taken from refs. (Gu *et al.* 2003; Haumann *et al.* 2003).

Figure 2 compares experimental (black lines) and calculated XANES spectra. In the case of the $[Ni(H_2O)_6]^{2+}$ complex, the convincing simulation (Fig. 2A, red) turned out to be relatively robust against minor variations in bond-lengths and –angles (data not shown). The experimental XANES spectrum of the *D. gigas* hydrogenase (Fig. 2B, black line) was first simulated using a model derived from the crystal structure which includes the complete Ni-Fe site and atoms up to ~5.5 Å around the Ni (see Fig. 2B, structure **1**). This simulation (Fig. 2B, green line) well reproduced the overall edge slope, maximum height, and shape. In a second step, a simplified model now including only direct ligands to the Ni appropriately capped by hydrogens (structure **2** in Fig. 2B) still yielded a reasonable simulation (Fig. 2B, blue line). This means that ligands at distances exceeding ~2.5 Å (e.g. the Fe, at ~2.9 Å) only marginally contribute to the edge spectrum. A third, even further simplified model, arranging the five Ni ligands in strict square-pyramidal geometry (Fig. 2B, structure **3**), is also in reasonable agreement with the experimental spectrum (Fig. 2B, red line). The simplifications of the model only led to a slight increase in the edge maximum, as predicted by model studies (Colpas *et al.* 1991). In summary, the used simulation code (FEFF 8.2 (Ankudinov *et al.* 1998)) is able to produce K-edge spectra of Ni compounds, which closely resemble the experimental data, provided that the Ni-ligand distances are well known from EXAFS analysis or crystallography.
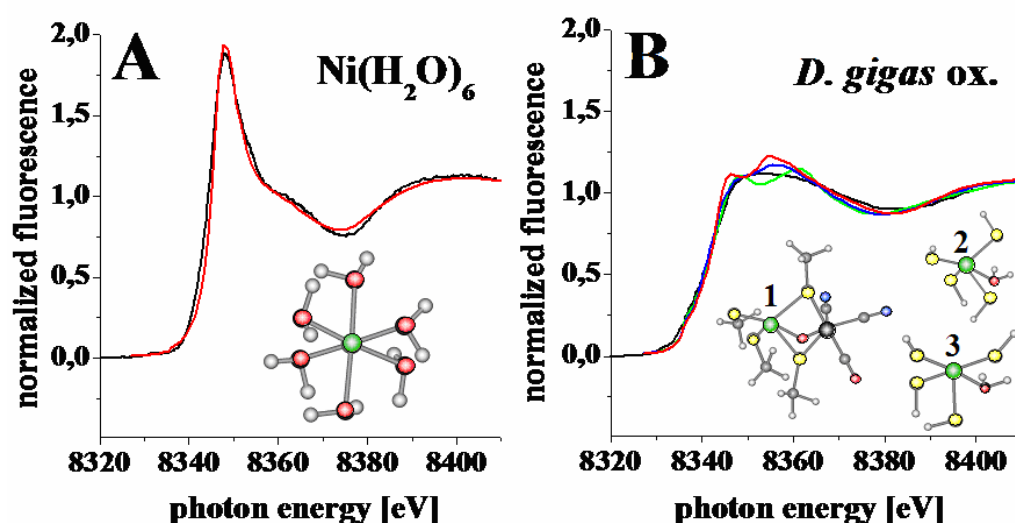
Figure 2: Comparison of experimental and simulated XANES spectra. (A) $[Ni(H_2O)_6]^{2+}$ complex (black, experimental data; red, calculated spectrum); (B) spectrum of the oxidized *D. gigas* hydrogenase (black, reproduced from ref. (Gu *et al.* 2003)). The simulation curves in (B) have been calculated on basis of the depicted structures (Ni, green; Fe, black; S, yellow; O, red; N, blue; C, grey; H, white) and are shown as a (1) green, (2) blue, and (3) red line. The Ni-ligand distances in the *D. gigas* hydrogenase here used in the simulations have been derived on basis of EXAFS analysis and taken from ref. (Gu *et al.* 2003). The Ni-Fe distance has not been assigned in EXAFS analysis of the oxidized *D. gigas* hydrogenase (Gu *et al.* 2003). Its value (2.9 Å) used in simulation (1) has been taken from the crystal structure (Volbeda *et al.* 1995).

These findings encouraged us to perform simulations of the Ni K-edge of the oxidized SH to verify the number of S-ligands to the Ni and to rule out some of the chemically different approaches, which provided similar fit qualities of the EXAFS spectrum. XANES simulations on basis of the Ni-ligand distances derived from the EXAFS fit approaches I, II, and VI (Table 4) involving only first-sphere ligands and assuming an almost octahedral Ni coordination geometry (see structures in Fig. 1C) are shown in Fig. 1A. The fit approaches I (C_1O_5) and II ($C_1O_1S_4$) produced XANES simulations (blue and green lines) which strongly deviate from the experimental spectrum (black). On the other hand, fit approach VI ($C_1O_3S_2$) produced a spectrum (Fig. 1A, red line), which is very similar to the experimental one. Exchanging the positions of the C,O,S ligands only marginally altered this result. Deviations from the octahedral site geometry and/or the inclusion of further atoms in the simulations (Fe and its ligands, capping methyl groups, additional S-ligands at distances between 2.5 and 3 Å from the Ni) produced spectra where the maximal magnitude of the K-edge was slightly reduced (data not shown).

We conclude: **(i)** Comparative XANES simulations on basis of alternative EXAFS fit results suggest the presence of an octahedral Ni in the oxidized SH, ligated by two thiols plus four C,O ligands. **(ii)** The presence of one CN ligand at the Ni is not uniquely indicated by, but clearly compatible with the XAS data.

A model for the Ni-Fe site in the oxidized SH

To construct a model of the Ni-Fe site of the oxidized SH, the above results of the EXAFS and XANES simulations that the Ni is ligated by only two thiols from cysteines plus four C/O atoms were taken into account. Furthermore, FTIR investigations revealed that an extra CN ligand is bound to Ni and Fe ([(CN)Ni-Fe(CN)$_3$(CO)] active site) (Happe *et al.* 2000; Bleijlevens *et al.* 2004; Van der Linden *et al.* 2004b). Chemical quantification revealed the presence of four CN molecules (Van der Linden *et al.* 2004b). That only one band in the CN region, therefore attributed to the CN at Ni, was shifted (see below and refs. (Happe *et al.* 2000; Bleijlevens *et al.* 2004; Van der Linden *et al.* 2004b)) whereas the other CN/CO bands, accordingly due to ligands at Fe, remained unchanged suggested that the charge density at the Fe was not altered and, hence, removal of a bridging oxide as found in standard hydrogenases seems not to occur in the SH under reducing conditions (see below). Conceivably, the two extra CN molecules block the bridging position in the SH. The lack of EPR signals from the active site indicates the presence of Ni^{II} and Fe^{II} oxidation states (see below). Which of the four thiols binding Ni in standard hydrogenases and also found in the SH are not ligated to Ni can not be deduced from the XAS data. It is a conservative assumption, which may lead to only moderate changes in the overall geometry of the Ni-Fe site, that two μ-CysS bridges between Ni and Fe are also present in the SH and that the other two thiols (terminal Ni ligands in standard hydrogenases) are not bound to Ni. (Alternatively, one of the bridging thiols may be replaced by an oxygen species and one of the other thiols then be a Ni ligand.) Where are the unbound thiols located? The Fourier-transform of the EXAFS oscillations of the oxidized SH shows a discernable peak in the region between 3 to 4 Å (see Fig. 1A, arrow; and Fig. 7A). Simulation of this peak with two sulphurs yields a Ni-S distance of ~3.65 Å, in agreement with these thiols being too far from Ni to be direct ligands. (We do not show the respective simulations because they are possibly not fully unique. Further scatterers like C-atoms from amino acids may also weakly contribute in the 3-4 Å distance range. The two remote cysteines may be in the thiol form (and linked via oxygen from water species or from amino acids to Ni) or, alternatively, may be present as oxidized thiolates (and linked via the respective oxygens to Ni).) A tentative model of the Ni-Fe site in the oxidized SH which is in agreement with the available XAS and FTIR data is shown in Fig. 3. With respect to the positions of S-ligands, the model represents one out of several possible arrangements (see also Discussion).
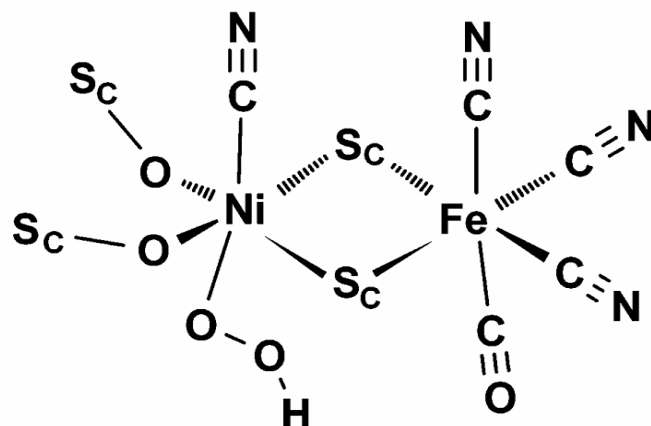
Figure 3. Working hypothesis for the structural features of the Ni-Fe site in the oxidized SH. Presumably, Ni and Fe both adopt a near-octahedral coordination geometry. The cysteine residues (represented as S_c) may be tentatively identified as C65 and C461 (bridging thiols) and C62 and C458. The latter two residues are assumed to be present as sulfenates with their oxygen atoms bound to nickel. This would be consistent with the estimated Ni-S distance of ~3.6 Å for two of the S-atoms. The ordering of the CN/ CO ligands at the Fe and the CN/OOH ligands at the Ni is arbitrary.

Structural changes at the Ni-Fe site of the SH induced by the substrates, NADH and H_2

Reductive activation of the oxidized SH, which is inactive in hydrogen cleavage, requires superstoichiometric concentrations of NADH or substoichiometric amounts of NADH in the presence of hydrogen. In former XAS work, drastic changes of the Ni K-edge and of the EXAFS oscillations have been observed (Gu *et al.* 1996; Müller *et al.* 1997) and EPR signals typical for the Ni-C (Ni^{III}) state emerged (Erkens *et al.* 1996) upon long-time incubation of samples with excess NADH. In our hands, the XAS spectra of most active SH samples treated with 10 mM NADH (under argon and in the absence of H_2) revealed small but reproducible changes (Fig. 4A,B, traces b) when compared to the ones of the oxidized enzyme (Fig. 4A,B, traces a). EPR measurements indicated the presence of the semiquinone form of FMN and reduced Fe-S clusters in the sample; a Ni-C EPR signal, however, was not detectable (Fig. 5). FTIR measurements revealed that the CN ligand to the Ni was retained if samples were treated with excess NADH; its $\nu(CN)$ band only shifted by 8 cm^{-1} to lower frequency (Bleijlevens *et al.* 2004; Van der Linden *et al.* 2004b).
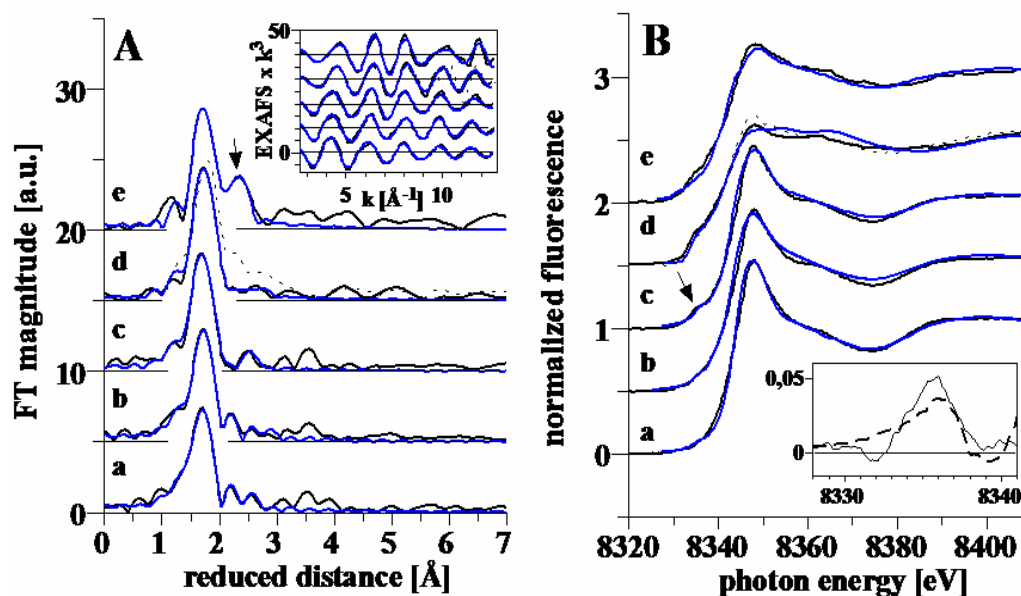
Figure 4: Activation and inactivation of the SH: XAS spectra and simulations. (A) Fourier-transforms of experimental EXAFS oscillations (black lines); the respective backtransforms (0-5 Å) are shown in the inset in the same order of spectra as in the main figure. (a) as-isolated, oxidized SH, (b) SH +NADH 10 mM, (c) SH +NADH 25 μM +H$_2$, (d) SH +dithionite 10 mM (+DTT 1 mM, dotted line), (e) aerobically isolated inactive SH preparation. The blue lines represent simulations according to the respective parameters listed in Table 5. The arrow highlights the second prominent peak in the FT. (B) Experimental XANES spectra (black; lettering as in A) and simulations (blue) calculated according to the respective Ni-ligand distances listed in Table 5 (for details see text). The arrow points to the additional peak feature in the K-edge observed in the presence of H$_2$. Spectra are plotted on the same scale and vertically displaced. Inset: Differences (NADH+H$_2$ – NADH) of experimental spectra (solid line) and of the corresponding simulations (dashed line).

The XANES spectrum of the NADH-treated SH showed a diminished primary maximum (Table 3) and increased intensity at low K-edge energies. The latter effect is attributable to $1s \rightarrow 4p_Z$ transitions shifting to lower energies and/or to enhanced s/p mixing of low-lying unoccupied molecular orbitals by which dipole-forbidden $1s \rightarrow 4s$ transitions gain oscillator strength upon a Ni-L$_6 \rightarrow$Ni-L$_5$ transition (ref. (Colpas *et al.* 1991; Dau *et al.* 2003) and references therein). The XANES features thus suggest the loss of one O-ligand, leading to a 5-coordinated Ni. Simulations of the EXAFS and XANES spectra of the NADH-treated SH, omitting one O-ligand (Table 5) and including slightly reduced Ni-O distances, are in agreement with the experimental data (Fig. 4A,B, traces a, blue lines). We conclude that upon reductive activation of the SH with NADH, one O-ligand is possibly reduced and released thereby preparing the Ni for

hydrogen binding by creating a vacant coordination site. The extra CN at the Ni is still present under these conditions (Bleijlevens *et al.* 2004; Van der Linden *et al.* 2004b).

Hydrogen cleavage occurs when the SH is incubated with only catalytic amounts of NADH under hydrogen. The XAS samples contained millimolar amounts of enzyme and only 25 µM NADH was used for activation. Full activation occurs as follows. Some SH molecules are reductively activated by the oxidation of the initially available NADH. These activated enzymes bind and cleave H_2 thereby regenerating NADH which, in turn, activates further SH molecules until the whole SH population is active. This autocatalytic activation of the enzyme produced a K-edge spectrum (Fig. 4B, trace c) which is overall similar to the one of the SH treated with NADH alone, but reveals a larger maximum. Interestingly, at the bottom of the rising part of the edge (at ~8336 eV, see arrow in Fig. 4B) a new peak feature emerged which is absent in the spectra of the oxidized and NADH-treated forms of the SH. This peak is most clearly seen in the difference spectrum (NADH+H_2 – NADH) (inset in Fig. 4B). Is the peak around 8336 eV a consequence of hydrogen binding to the Ni? FTIR measurements revealed that the CN-ligand is preserved in the presence of hydrogen and catalytic amounts of NADH.

Its v(CN) stretching band shifts, however, dramatically (from 2098 to 2051 cm^{-1}), while the stretching frequencies of the diatomic ligands bound to Fe did not change. The shift has been proposed to be due to the binding of hydrogen to nickel (Happe *et al.* 2000; Van der Linden *et al.* 2004b). From fits of the NADH+H_2 EXAFS spectrum (Fig. 4A, trace c) using a $(H_1)C_1O_2S_2$–coordination of the Ni (the H atom has not been explicitly included in the EXAFS fit because its backscattering amplitude is negligible) similar parameters as in the NADH-treated SH were obtained. The simulation of the XANES spectrum of the NADH+H_2-treated sample on basis of the EXAFS bond lengths summarized in Table 5 and now explicitly including a H atom at 1.7 Å distance from the Ni properly reproduced the experimental spectrum (Fig. 4B, trace c, blue line) including the peak feature at 8336 eV. A peak at ~8336 eV is observed in the difference spectrum of the simulations (inset of Fig. 4B, dashed line) which matches the experimental difference spectrum. Thus, the XANES spectra are compatible with the notion that, in the NADH+H_2-treated SH, hydrogen binds to the Ni.

The Ni-C state of the SH

In previous studies, a Ni-C EPR signal has been reported in the SH under strongly reducing conditions (Erkens *et al.* 1996; Schneider *et al.* 1996; Bleijlevens 2002), however, only in a relatively narrow range of redox potentials (-350 mV < E_0 < -250 mV) (Erkens *et al.* 1996). At lower potentials, the Ni again becomes EPR silent, explainable by a more reduced state containing Ni^{II} (Erkens *et al.* 1996).

Under conditions leading to maximal H_2 cleavage activity (50 mM Tris-HCl, pH 8) (Keefe *et al.* 1995), only small changes of the XAS spectra were induced by the natural substrates, NADH and H_2; no Ni-C EPR signal was detectable (see Fig. 5). A Ni-C signal was absent also after incubation at various NADH: NAD ratios to vary the redox potential in the absence or presence of H_2 (data not shown).
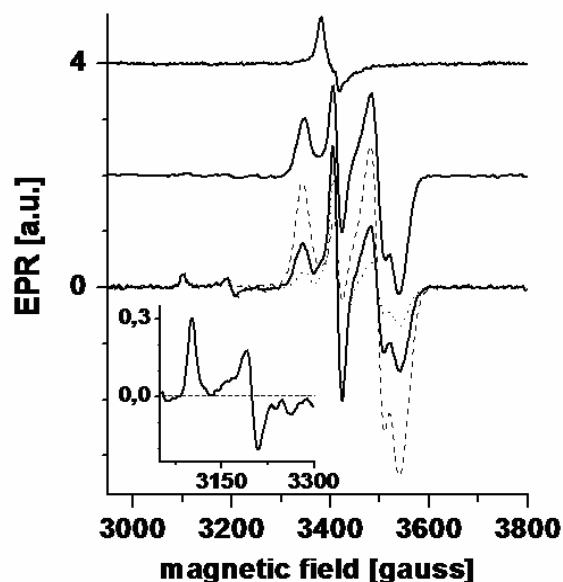

Figure 5: EPR spectra of the SH under various redox conditions. Top: as-isolated enzyme (pH 8); middle: enzyme reduced with NADH (10 mM, pH 8); bottom: enzyme reduced with dithionite (10 mM, pH 8; solid line), NADH (10 mM, pH 6; dashed line), or dithionite (10 mM, pH 6; dotted line). The inset shows an expansion of the low field region of the Ni-C signal of the spectrum obtained with dithionite at pH 8. EPR conditions: microwave power 1 mW, temperature 30 K. Spectra have been normalized according to the protein concentrations in the samples. The spin concentration of the Ni-C signal was 13 % of that of the [2Fe-2S] signal in the same spectrum as obtained by computer simulation and double integration as described in ref. (Van der Linden *et al.* 2004a).

A sample of the oxidized SH that was incubated with 10 mM dithionite ($E_0^{'}$ = -590 mV) (Mayhew 1978) for 10 min at pH 8 revealed a small Ni-C signal (Fig. 5); its spin concentration was 13 % of that of the [2Fe-2S] cluster in the same sample. The spin concentration of the [2Fe-2S] cluster in the NADH-reduced enzyme was assumed to be equal to the enzyme concentration as reported in ref. (Van der Linden *et*

al. 2004a). As the dithionite-induced Fe-S signal was about half that induced by NADH, this means that the Ni-C signal amounts to about 5-10 % of the enzyme concentration in the dithionite-treated sample. The XANES spectrum of the latter sample (Fig. 4B, trace d) drastically differs from the one of the oxidized SH in showing a pronounced shoulder in the rising part of the edge and a primary maximum that is diminished to a value close to one (Table 3). Such K-edge properties are typical for compounds where the Ni is coordinated by four sulphur ligands (Haumann *et al.* 2003), (Colpas *et al.* 1991), (Eidsness *et al.* 1988) Thus, a structural change of the Ni site seemingly is caused by strongly reducing conditions.

A XANES spectrum with somewhat higher maximum and less pronounced shoulder was observed (see Fig. 4, dotted lines) in a sample treated with the weaker reductant dithiothreitol (DTT, E_0 = -330 mV); in this sample no Ni-C signal could be detected. Very similar XANES spectra as in the dithionite-treated SH were also observed at pH 6 where the hydrogen cleavage activity of the SH after activation is very low.(Keefe *et al.* 1995) At pH 6, in the presence of 10 mM NADH, a Ni-C EPR signal of similar extent as above was detected (see Fig. 5).

At the lower potential induced by 10 mM dithionite at pH 6 a negligible Ni-C signal was obtained (Fig. 5). In our hands, a quantitative population of the Ni-C could not be induced also by any further redox treatments using different combinations of NADH and NAD or dithionite under H_2 at pH values ranging between 6 and 8. That similar XANES spectra were obtained under various reducing conditions suggests a similar gross structure of the Ni site. This modified side may carry additional (H,(CN),O) ligands in its most oxidized state, in the Ni-C state, and in its most reduced state (see below).

In Fig. 4A (trace d) the FT of the EXAFS spectrum of the dithionite-treated SH is shown. Notably, the peaks between 3 and 4 Å, attributed to the two remote thiols in the oxidized SH, are absent. The respective EXAFS oscillations (Fig. 4A, inset, trace d) reveal larger amplitudes at higher *k*-values than the ones of the oxidized and NADH/ NADH+H_2 treated samples, which are expected if the EXAFS is dominated by contributions from higher-*Z* backscatterers, e.g. sulphur ligands to the Ni, in line with the XANES spectrum. The simulation of the EXAFS spectrum is complicated by the likely presence of a mixture of states (see above). A reasonable simulation (Fig. 4A, trace d, blue line), however, is already obtained using only four sulphur ligands to the Ni arranged in two shells at mean distances of 2.2 and 2.5 Å and one Ni-Fe vector (Table 5). Addition of a further (CN)/O-ligand did not improve the fit. In Fig. 4B (trace d) a simulation of the XANES on basis of the EXAFS parameters in Table 5 is shown (blue line), representing a H_1S_4-coordinated Ni site (square-pyramidal geometry with one longer Ni-S distance out of plane; H at 1.7 Å from Ni). This simulation well reproduced the edge maximum and shoulder. A higher maximum and a less pronounced shoulder were obtained if the H was replaced by O (not shown).

Interestingly, we obtained a similar XANES spectrum (Fig. 4B, trace e) as in the DTT-treated SH (Fig. 4B, trace d, dotted line) in a preparation where catalysis was largely impaired (specific activity of only 9 U/mg after reductive activation compared to 61 U/mg in the control samples). The XANES spectrum of this SH preparation (further on termed inactive SH) in its oxidized form (Fig. 4B, trace e) was practically unchanged if H_2, NADH, NADH+H_2, or dithionite were added. Under reducing conditions, EPR measurements indicated the presence of the FMN semiquinone; the observed EPR signals in the g = 1.94 region differed from the ones in the native enzyme (see last Results section for more details). A Ni-C signal, however, was not observed under any of the tested conditions. FTIR revealed the lack of the CN ligand at the Ni (not documented).

The EXAFS Fourier-transform of the inactive SH shows a well resolved peak at ~2.5 Å (arrow in Fig. 4A, trace e), which is also present, to some extent, in the DTT-treated enzyme, but absent in the oxidized samples. The EXAFS of the inactive SH is also rather similar to the ones from the reduced *D. gigas* (Gu *et al.* 1996; Gu *et al.* 2003) and *A. Vinosum* (Davidson *et al.* 2000) hydrogenases. Indeed, the best simulation of the EXAFS spectrum of the inactive SH is obtained using four sulphur ligands to the Ni (Table 5). The inclusion of a further oxygen ligand is optional. The longer Ni-S distances and the Ni-Fe vector (with ~2.6 Å length much shorter than the ~2.9 Å found in the native oxidized SH) both contribute to the new peak in the FT. A simulation of the XANES using a O_1S_4 coordination of the Ni produced an edge (not shown) with a maximum that was too small compared to the experimental spectrum. However, the inactive sample showed a residual activity of ~16 % of the control. Adding 16 % of the simulated spectrum of the native oxidized SH to the O_1S_4 simulation now produced a XANES spectrum (Fig. 4B, trace e, blue line), which is in good agreement with the experimental spectrum of the inactive SH.

In summary, when the hydrogen cleavage activity of the SH is low (in inactive preparation**s** or after activation of native preparations at pH 6) and when the reverse reaction, hydrogen formation, is enforced (e.g. in the presence of high amounts of strong reductants or at pH 6) the Ni coordination is drastically changed. Then, the two sulphur ligands that are more remote from the Ni in the native enzyme apparently become direct Ni ligands. Thereby, a Ni-XS_4 site is formed which seems to closely resemble the one in standard hydrogenases. The XAS and EPR results may be rationalized, in analogy to the situation in standard hydrogenases, by assuming that in the modified Ni-XS_4 site, X is either an oxygen ligand or absent in its more oxidized state, and possibly a hydrogen species in the Ni-C and more reduced states. Seemingly, neither the Ni-C state, nor the Ni-XS_4 site are involved in the hydrogen cleavage reaction by the SH.

Table 5.   EXAFS fit parameters of SH preparations under various redox conditions[a]

sample	shell	N_i [per Ni]	R_i [Å]	σ^2_i [Å²] x10³	R_F (1-3 Å) [%]
WT oxidized	C	1	2.00	1.0	6.3
	O	3	2.05	7.0	
	S	1	2.24	1.5	
	S	1	2.43	5.6	
	Fe	1	2.88	13.0	
WT +NADH	C	1	1.98	1.0	8.1
	O	2	2.03	2.5	
	S	1	2.23	1.5	
	S	1	2.45	5.2	
	Fe	1	2.60	10.2	
WT +NADH +H₂	[H]	[1]	[nd]	[nd]	9.2
	C	1	1.98	1.0	
	O	2	2.02	2.0	
	S	1	2.22	1.5	
	S	1	2.43	7.0	
	Fe	1	2.55	8.5	
WT +dithionite / +DTT	[H] / O,C	[1] / 1	[nd] / 1.99	[nd] / 1.0	9.5 / 14.5
	S / S	3 / 2	2.15 / 2.20	4.0 / 4.1	
	S / S	1 / 2	2.49 / 2.52	4.9 / 3.0	
	Fe / Fe	1 / 1	2.53 / 2.60	7.7 / 4.0	
WT inactive	O	1	1.98	1.0	14.9 13.5
	S S	2 2	2.16 2.18	1.5 2.7	
	S S	2 2	2.41 2.47	15.2 12.3	
	Fe Fe	1 1	2.55 2.57	2.0 3.0	
I64A all conditions	O	4	2.05	3.2	7.8
	S	1	2.26	4.2	
	S	1	2.48	6.5	
	Fe	1	2.98	11.7	
L118F oxidized +NADH / NADH+H₂	C	1	1.89	1.0	11.3
	C / C	(1 / 1)	1.90 / 1.85	1.0 / 1.0	13.3 / 11.0
	O	2	2.11	1.9	
	O / O,[H]	1 / 1,[1]	2.06 / 2.02,[nd]	1.0 / 1.0,[nd]	
	S	2	2.16	1.7	
	S / S	2 / 2	2.15 / 2.19	7.0 / 4.8	
	S	1	2.29	3.4	
	S / S	1 / 1	2.27 / 2.54	7.2 / 4.0	
	Fe	1	2.72	15.0	
	Fe / Fe	1 / 1	2.70 / 2.62	12.2 / 14.6	

[a]For the I64A mutant, the same parameters apply for the oxidized, NADH-, and NADH+H₂-treated states; the respective R_F-values are similar (±0.5 %). Where hydrogen has been assumed to be bound to the Ni (in the presence of NADH+H₂), the (H) has not been included in the EXAFS simulations (nd).

Structural models for the Ni site after activation, reduction, and inactivation of the SH

We summarize the changes in Ni coordination induced by activation under NADH and H_2 and by stronger reductive treatments and in the inactive SH preparation in Fig. 6. (It is worth to note that the presence (or absence) of the CN ligand is in line with previous observations (Happe *et al.* 2000; Bleijlevens *et al.* 2004; Van der Linden *et al.* 2004b) and the presented FTIR results (see Fig. 8); the CN ligand improved the respective XAS simulations in all cases where it is shown in Fig. 6.) Likely, only the structures of the Ni site in the oxidized (1), NADH- (2) and NADH+H_2-treated SH (3) represent intermediates of the hydrogen cleavage cycle in the native enzyme. The modified Ni site (4), which seems to be similar to the one in standard hydrogenases, is formed during inactivation of the SH and under strongly reducing conditions.
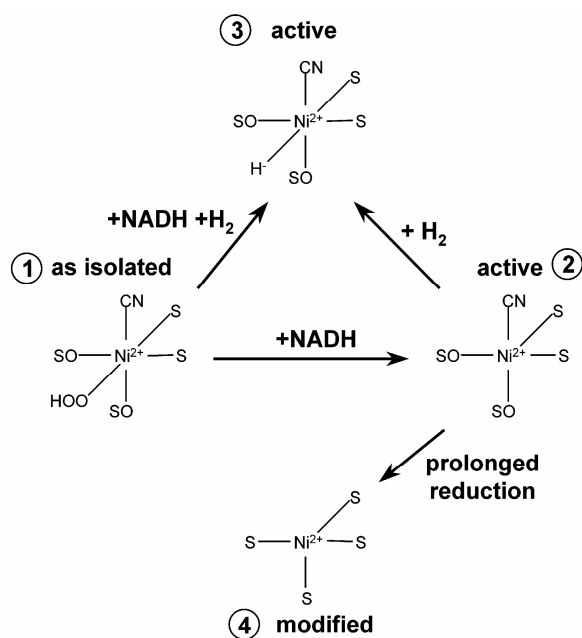

Figure 6: Tentative scheme for the structural changes inducible at the Ni site of the SH. Structure (1), oxidized state of the native SH. By reduction with NADH the SH is activated yielding state (2); one oxygen ligand is removed from the Ni. The active state (3), which seemingly contains bound hydrogen, is observed under autocatalytic conditions (catalytic amounts of NADH under hydrogen). Prolonged reduction leads to a strongly modified Ni site (4) where four S-ligands are bound to Ni (additional O-ligand(s) may be present) and the Ni-C (Ni^{III}-H$^-$) state can be formed. A similar structure (4) is observed in catalytically inactive SH protein already in its aerobically isolated form. The presence of the CN at Ni in structures 1, 2, and 3 is in agreement with FTIR results (Happe *et al.* 2000; Bleijlevens *et al.* 2004; Van der Linden *et al.* 2004b).

The Ni site in an inactive and in an oxygen-sensitive SH mutant

Two main types of SH enzymes generated by site-directed mutagenesis are of particular interest: Mutants forming tetrameric SH protein that is either (1) catalytically inactive or shows (2) hydrogen-oxidizing activity, but is sensitive to inhibition by oxygen. In the I64A mutant, HoxH-isoleucine-64 was replaced by alanine, resulting in an enzyme that is inactive in both the H/D exchange reaction and H_2 oxidation. In the L118F mutant, HoxH-leucine-118 was replaced by phenylalanin; hydrogen cleavage activity is inhibited by oxygen (Burgdorf *et al.* 2002).
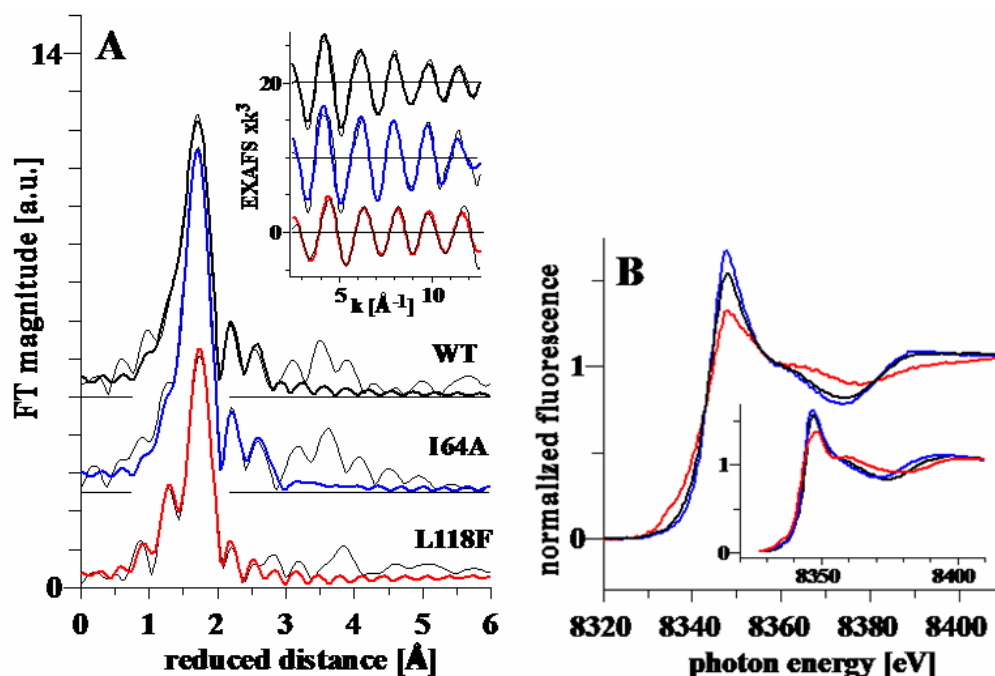
Figure 7: Comparison of XAS spectra of wild type SH and of two mutants, I64A and L118F. (A) Fourier-transforms of experimental EXAFS oscillations of the oxidized enzymes (black thin lines) and simulated spectra (thick lines). Note the peaks at reduced distances of 3-4 Å. Inset: backtransforms (0-5 Å) of the experimental spectra and the respective simulations. (B) Experimental XANES spectra of wild type SH (black), the I64A (blue), and L118F mutant (red); the inset shows the respective simulated XANES spectra using only first shell ligands to the Ni and Ni-ligand distances as listed in Table 5.

XAS reveals that in the oxidized I64A mutant, both the maxima of the K-edge (Fig. 7B, blue line; Table 3) and of the main peak of the FT (Fig. 7A, middle trace) are larger than in the wild type, pointing to a more homogenous distance distribution in the ligand environment of the Ni. The respective FTIR spectrum lacks the band at 2097.6 cm^{-1} (Fig. 8, arrows), which is observed in the wild type and there attributable to the CN at Ni. (The presence of several bands in the CO region in I64A points to limited heterogeneity at the Fe site.) The XAS spectra are well simulated (Fig. 7, A and B, blue lines) assuming a O_4S_2 Ni-coordination (Table 5); the XAS data shows no indications for heterogeneity at the Ni site. NADH and NADH+H_2 did not change the XAS spectrum (data not shown); seemingly the Ni coordination is not affected by activating conditions in the I64A mutant.

The XANES spectrum of the oxidized L118F mutant (Fig. 7B, red line) reveals a greatly diminished maximum and increased intensity in the low-energy region; the main FT peak (Fig. 7A, lower trace) is diminished and shifted to higher distances and peaks in the 3-4 Å region are smaller compared to the wild type. The FTIR spectrum (Fig. 8) reveals four absorption bands in the CN frequency range similar to the wild type. The relative intensities of these absorption bands differ; small frequency shifts are observed. Slightly altered charge distributions at the Ni and Fe and/or the loss of the CN in a fraction of the enzyme population may account for these effects**.** Upon reduction of L118F by NADH+H_2, the band attributed to the CN at the Ni shifted by 44 cm^{-1} to lower frequencies, similar to the wild type where this shift is 47 cm^{-1} (data not shown). Seemingly, in the L118F mutant the CN ligand at the Ni is preserved at least in part of the enzyme population.

Both the XANES (inset in Fig. 7B, red line) and EXAFS spectra (Fig. 7A, lower trace) were well simulated assuming a $C_1O_2S_3$ Ni-coordination (Table 5); pointing to the binding of an additional sulphur to the Ni. (It can not be excluded that the apparent coordination of Ni by three sulphurs results from a heterogeneous enzyme population where both Ni-S_4 and Ni-S_2 species are present.)
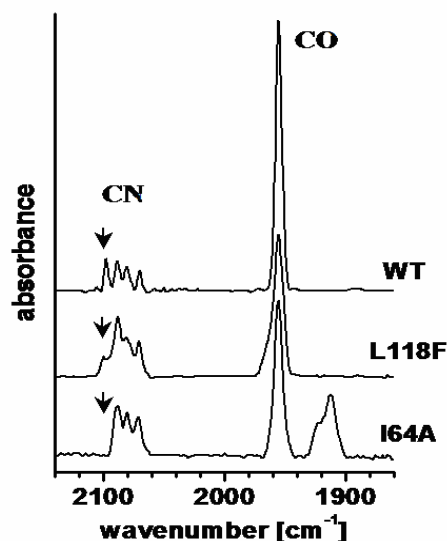
Figure 8: FTIR spectra of wild type SH (WT) and L118F and I64A proteins (oxidized forms). Spectra are not normalized and vertically displaced for comparison. The absorption bands in the 2100 to 2050 cm^{-1} frequency region are due to CN groups; the band at ~1955 cm^{-1} is due to the CO bound to the Fe atom (Happe *et al.* 2000; Van der Linden *et al.* 2004b). The band at 2098 cm-1 in the oxidized wild type SH (arrow) is attributed to a CN bound to the Ni.(Van der Linden *et al.* 2004b) It shifts to 2051 cm^{-1} with NADH+H$_2$ (Happe *et al.* 2000; Van der Linden *et al.* 2004b). In the L118F mutant, the respective band at 2099 cm^{-1} in the oxidized enzyme is shifted to 2055 cm^{-1} with NADH+H$_2$ (not shown). In the I64A mutant, the band attributable to the CN at the Ni is seemingly absent.

In the presence of 10 mM NADH, the decrease of the main peak in the FT of L118F (Fig. 9, dotted line) is compatible with the loss of one oxygen ligand from the Ni (Table 5). With catalytic amounts of NADH in the presence of H$_2$ a similar peak as in the wild type around 8336 eV appeared in the K-edge (Fig. 9, inset) and the main FT peak was shifted (Fig. 9, dashed line). The EXAFS was simulated using a C$_1$O$_1$S$_3$ Ni-coordination, but with longer Ni-S distances than in the NADH-treated enzyme (Table 5). In analogy to the wild type SH, the XANES may indicate hydrogen-binding to the Ni in L118F under NADH+H$_2$.
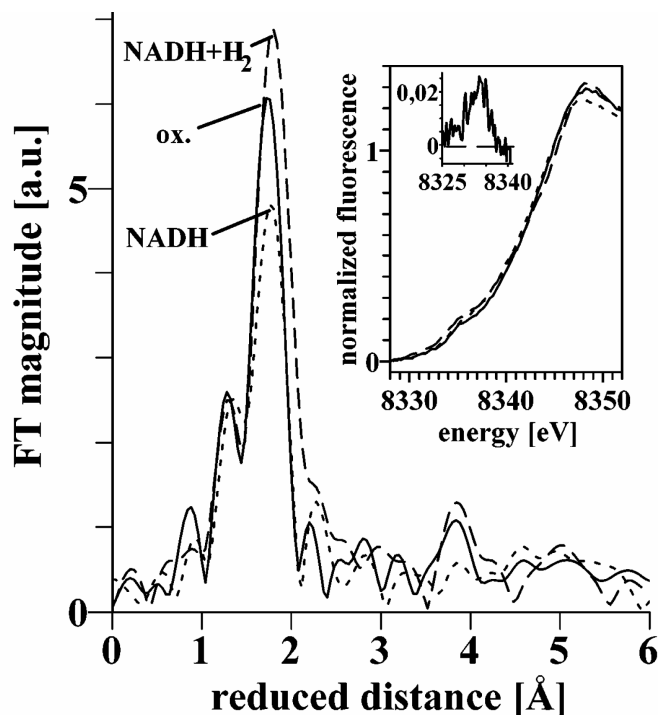
Figure 9: Fourier-transforms of EXAFS oscillations of the L118F mutant of the SH in the oxidized (solid line), NADH- (dotted line), and NADH+H$_2$-treated states (dashed line). The inset shows the respective K-edge spectra. The small figure in the inset represents the difference spectrum (NADH+H$_2$ – NADH), respectively.

In summary, both mutants reveal changes at their Ni sites. One interpretation of XAS and FTIR data is the exchange of the CN at the Ni against oxygen in I64A. In L118F, the CN at the Ni is preserved at least in a fraction of the enzyme; the XAS data is compatible with an additional thiol bound to the Ni. Both mutant preparations may be heterogeneous according to the FTIR data; either with respect to the coordination of at least the Fe in I64A or, to some extent, of the Ni in L118F.

Redox reactions in wild type and mutant SH enzymes studied by EPR

To investigate whether the different structures of the Ni sites in the native, inactive, and mutant enzymes affected the redox properties of the cofactors (Ni-Fe, Fe-S clusters, FMN), EPR spectra were recorded of oxidized samples and after addition of catalytic amounts of NADH in the presence of H$_2$. In all oxidized enzymes, spectra similar to that of the native enzyme (see Fig. 5) were obtained (data not shown), which indicate the

same oxidation of the redox cofactors as in native enzyme after aerobic purification (Albrecht 1994; Schneider *et al.* 1996; Happe *et al.* 2000). The EPR spectrum of the native, $NADH+H_2$ treated enzyme (Fig. 10, top trace) has been attributed to the overlay of an isotropic EPR signal centered at g ~2.00 (arrow in Fig. 10) due to FMN in the semiquinone form and two or more anisotropic signals from reduced Fe-S clusters (Erkens *et al.* 1996; Schneider *et al.* 1996; Happe *et al.* 2000). Comparison with the spectra at 30 K (Fig. 5) shows that the spectrum is an overlay of at least two anisotropic signals: one of a reduced $[2Fe-2S]^+$ cluster, also detectable at 30 K, and one of a signal from one or more rapidly relaxing $[4Fe-4S]^+$ clusters (detectable by the line at g = 1.86), in agreement with ref. (Schneider *et al.* 1996). The latter signal cannot be observed at higher temperatures due to relaxation broadening.

Midpoint potentials for the single electron reduction of the bound FMN (E_0 = ~-200 mV); of the [2Fe-2S] cluster of the diaphorase unit of the SH (E_0 = -325 mV); and of the [4Fe-4S] cluster(s) (-385 mV < E_0 < -445 eV) have been reported (Erkens *et al.* 1996; Schneider *et al.* 1996). Thus, in the presence of 25 μM NADH (E_0 = -320 mV) the FMN and the [2Fe-2S] cluster in the enzyme (at a concentration of ~1 mM) are expected to become only partly reduced. Because of their low redox potentials, the [4Fe-4S] clusters are not reduced under these conditions. They may, however, become (partly) reduced in the presence of excess NADH (compare Fig. 5). With substoichimetric concentrations of NADH in the presence of H_2, reduction of the [4Fe-4S] clusters is expected to occur preferentially by electrons derived from hydrogen cleavage at the Ni-Fe cofactor after its reductive activation. The observation of the g_x-line at 1.86 (Fig. 10, top) may thus be taken as an indicator for the reductive activation and subsequent hydrogen cleavage at the Ni-Fe site, which readily function in the native SH.
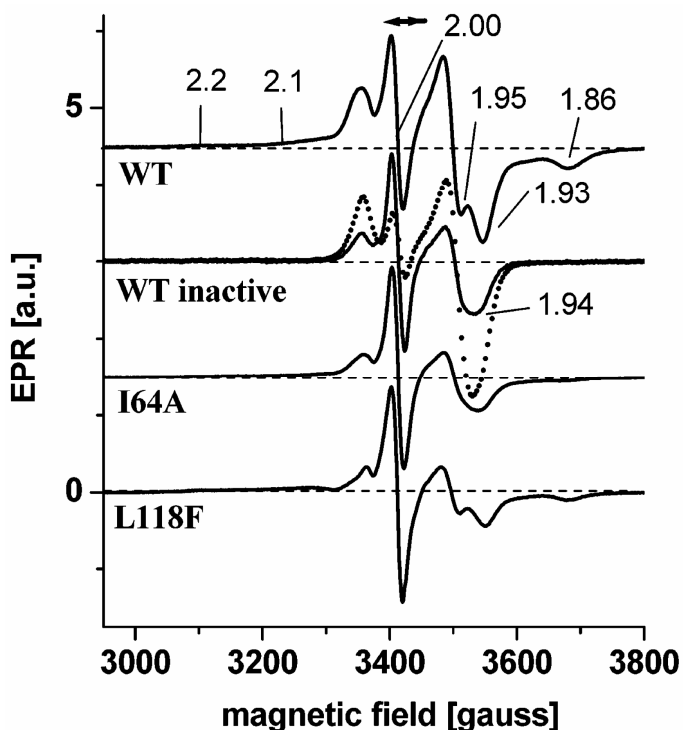
Figure 10: EPR spectra of the wild type (WT) native and inactive SH and of two mutants in their NADH+H$_2$-treated states. EPR conditions: microwave power 0.25 mW, temperature 10 K. Spectra have been normalized to the signal attributed to FMN semiquinone at g = 2 (arrow) and vertically displaced. The spectra shown as solid lines were obtained from SH samples incubated with 25 µM NADH under hydrogen at pH 8. The spectrum shown as a dotted line was measured on a sample of the inactive SH in the presence of 10 mM dithionite. Numbers indicate approximate g-values.

In the inactive SH preparation under similar conditions, the FMN semiquinone signal was also detected (Fig. 10). However, the $g_x = 1.86$ line of the reduced [4Fe-4S] cluster(s) is missing and the line shape of the [2Fe-2S]$^+$ signal (around g = 1.95/1.93) has noticeably changed. Even in the presence of 10 mM dithionite (Fig. 10, dotted line) no reduced [4Fe-4S] clusters were observable. There are two possible explanations for these observations: (a) the inactive SH does not operate in the hydrogen-cleavage direction necessary to generate electron transfer between the Ni-Fe and [4Fe-4S] cofactors; (b) the cubane clusters have been affected such that they can no longer be detected as normal reduced [4Fe-4S] clusters.

In the NADH+H$_2$-treated I64A mutant, the shape of the EPR spectrum (Fig. 10) is similar to the one of the inactive enzyme. Only FMN-semiquinone signal and a

modified signal from the [2Fe-2S]$^+$ cluster are present; [4Fe-4S]$^+$ signals were not observed. The XAS spectrum of I64A was unchanged under NADH or NADH+H$_2$. The EPR and XAS data are compatible with the notion that the activation process of the Ni-Fe cofactor is impaired in the I64A enzyme; electron transfer from the Ni-Fe cofactor to the [4Fe-4S] clusters may not occur.

In the L118F mutant, an EPR spectrum of similar shape as in the native SH was obtained under NADH+H$_2$ (Fig. 10). Compared to the wild type, the relative magnitudes of the overlayed signals were changed, pointing to altered redox equilibria between cofactors and/or to a heterogeneous enzyme population. However, the same cofactors as in the native enzyme become reduced in a sizable fraction of the L118F preparation.

In the presence of catalytic amounts of NADH under hydrogen, a Ni-C EPR signal (due to Ni^{III}-H$^-$,(Happe *et al.* 2000; Lubitz *et al.* 2002; Müller *et al.* 2002; Brecht *et al.* 2003; Foerster *et al.* 2003) emerging around g = 2.1-2.2, and expected to be visible at 10 K because of negligible spin coupling (Erkens *et al.* 1996) between Ni^{III} and [Fe-S]$^+$) was absent, indicating a Ni^{II} oxidation state under hydrogen-cleavage conditions.

Discussion

Hydrogen cleavage at the unusual Ni-Fe site of the SH: Some mechanistic implications

Standard Ni-Fe hydrogenases have a (CysS)$_2$Ni(μ-O)(μ-CysS)$_2$Fe(CN)$_2$(CO) active site. For the NAD-reducing, cytoplasmatic Ni-Fe hydrogenase (SH) from *Ralstonia eutropha* a (CysS)$_2$(CN)(O)Ni(μ-CysS)$_2$Fe(CN)$_3$(CO) site was proposed on basis of infrared studies (Happe *et al.* 2000; Bleijlevens *et al.* 2004; Van der Linden *et al.* 2004b). (Compared to standard hydrogenases, an extra CN seems to be bound to both Ni and Fe in the SH.[43, 49, 112] Chemical quantification revealed the presence of four CN molecules.[49] One FTIR band in the CN region (at ~2098 cm^{-1}) disappeared when one CN was specifically removed from the SH by chemical treatments as revealed by CN quantification[49] and the same band was absent in a mutant where one of the auxiliary maturation proteins of the Ni-Fe site was deleted.[112] Only the 2098 cm^{-1} band shifted when the SH becomes reduced.[43, 49, 112] Under all conditions, the other CN bands, attributable to three CN molecules according to simulations of FTIR spectra of the CN region, were unchanged.[43, 49, 112] These observations suggest that the 2098 cm^{-1} band is due to CN bound only to Ni (see also Fig. 8). The absence of shifts of ν(CN)$_{Fe}$ under conditions where the Fe-S clusters become reduced suggest that the other extra CN is bound to the Fe of the Ni-Fe cofactor (Bleijlevens *et al.* 2004; Van der Linden *et al.*

2004b). A bridging CN between Ni and Fe has been discussed in the context of standard hydrogenases (ref. (Siegbahn *et al.* 2001) and references therein), but not observed experimentally. Such a species seems to be difficult to reconcile with the results outlined above, namely that one CN can be specifically removed whereas the FTIR frequencies of the other three CN ligands remain unaffected. Removal of a bridging CN may be expected to alter the FTIR frequencies of Fe-bound CN/CO which is not observed (Bleijlevens *et al.* 2004; Van der Linden *et al.* 2004b). A bridging CN may not fully be excluded but clearly represents a less likely option.) The coordination of four Cys residues to Ni proposed in refs. (Happe *et al.* 2000; Van der Linden *et al.* 2004b) was, however, only based on the presence of four conserved Cys residues in the HoxH subunit (Tran-Betcke *et al.* 1990).

In this work, for the first time, complementary simulations of XANES and EXAFS spectra supplemented by FTIR and EPR measurements were employed to deduce the structural and electronic properties of the Ni site. The results demonstrate that the Ni coordination in the SH strongly differs from that in standard hydrogenases. In the oxidized inactive enzyme the divalent Ni is coordinated by only two cysteine residues, three oxygens, and one cyanide in a near-octahedral coordination geometry ($Ni^{II}(CN)_1O_3S_2$). Two sulphur bridges between Ni and Fe as in standard hydrogenases are compatible with, but not uniquely implied by the XAS data. The remaining two conserved cysteines of the SH are placed more remote from the Ni (estimated Ni-S distance ~3.65 Å). Accordingly, we propose a $(CysS)_{0-1}(CN)(O)_3$ $Ni(\mu\text{-}CysS)_{2-1}Fe(CN)_3(CO)$ active site in the oxidized SH. Presumably, the extra CN ligands at Ni and Fe block the bridging position between the Ni and Fe atoms. Although being pronouncedly different from standard hydrogenases, embedment of the altered Ni-Fe cofactor in its binding cavity of the SH may require only subtle amino acid rearrangements with respect to the situation in, i.e., the *D. gigas* structure (Volbeda *et al.* 1995; Volbeda *et al.* 1996) because (i) only few amino acids actually coordinate the Ni and Fe atoms due to their binding of four CN and one CO ligands and (ii) all four cysteine residues are still relatively close to Ni (Ni-S distances between 2.24 and 3.65 Å).

We have obtained evidence that the reductive activation of the SH with NADH causes the detachment of one oxygen ligand from the Ni thereby creating an open binding site with $Ni^{II}(CN)_1O_2S_2$ coordination. Because the frequencies of the FTIR bands attributed to CN/CO at Fe do not shift upon its removal (Bleijlevens *et al.* 2004; Van der Linden *et al.* 2004b), it seems to be unlikely that this oxygen species is bound in a bridging position between Ni and Fe as found in standard hydrogenases. Rather, a terminal oxygen seems to be lost. It is straightforward to assume that a hydrogen species is subsequently bound to the open site yielding the $Ni^{II}H_1(CN)_1O_2S_2$ state. Presumably, this state represents an early intermediate in the reaction cycle of the SH.

In standard Ni-Fe hydrogenases (and in the *D. baculatum* Ni-Fe-Se hydrogenase) the active state is the Ni-C state as identified by its characteristic S = ½ EPR signal attributable to a formal Ni^{III} oxidation state (Happe *et al.* 2000; Lubitz *et al.* 2002; Müller *et al.* 2002; Brecht *et al.* 2003; Foerster *et al.* 2003). It was long known that this state involved a light-sensitive hydrogen species (Van der Zwaan *et al.* 1985). Recent EPR studies indicated that this is a hydride bound in a bridging position between the Ni and Fe atoms (Brecht *et al.* 2003). DFT calculations yielded several detailed mechanistic schemes for the turnover of hydrogen at the Ni-Fe cofactor in standard hydrogenases, all involving a Ni-C (Ni^{III}-H^-) state (Amara *et al.* 1999; Niu *et al.* 1999; Siegbahn *et al.* 2001; Stein *et al.* 2002). The Ni-C state has long been considered a key intermediate of hydrogen turnover (Van der Zwaan *et al.* 1987; Fan *et al.* 1991; Coremans *et al.* 1992a). However, in the SH, the Ni-C state seems not to be involved in the catalytic cycle of hydrogen cleavage as it is not observed when the SH is highly active. This result of the present study is in agreement with previous findings (Erkens *et al.* 1996; Schneider *et al.* 1996; Happe *et al.* 2000; Van der Linden *et al.* 2004a; Van der Linden *et al.* 2004b).

What prevents the formation of the Ni-C state in the hydrogen cleavage reaction of the SH? Thiolates are electron-rich, polarizable ligands that stabilize higher oxidation states of nickel thereby bringing the redox potential into the physiologically relevant range (Nag 1980; Haines *et al.* 1981; Fox *et al.* 1990; Maroney 1999). Thus, the predominant coordination of the Ni by hard (O,C) ligands found in the native SH stabilizes the Ni^{II} state. Likely, a further stabilization of Ni^{II} is obtained by the CN ligand favouring the low spin, low oxidation state (Reissmann *et al.* 2003) by its good π-donor properties. Presumably, for the same reason there are the CN/CO ligands (DeLacey *et al.* 1997; Pierik *et al.* 1999) at the Fe in the Ni-Fe hydrogenases. In the SH, the Fe coordination seems to be saturated by one CO and three cyanides, one thiol, and one S/O ligand (Happe *et al.* 2000; Van der Linden *et al.* 2004b), rendering a bridging hydride species unlikely, if not impossible. Thus, redox chemistry involving H_2 may be restricted to the less oxidizable Ni site and does not involve a Ni-C state with a Ni^{III}-H^- species.

XAS measurements at the Ni L-edge (Wang *et al.* 2000; Wang *et al.* 2001a; Wang *et al.* 2001b) and DFT calculations (Fan *et al.* 2002) suggest that high-spin Ni^{II} is present in the reduced state of standard hydrogenases. Accordingly, L-edge spectra of reduced *D. gigas* hydrogenase show moderately resolved multiplet features on the L_3- and L_2-edges (weak splitting of the edge peaks), typical for more covalently, i.e. sulphur-bound high-spin Ni^{II} (Van Elp *et al.* 1994; Wang *et al.* 2000; Wang *et al.* 2001a; Wang *et al.* 2001b) . The oxidized SH shows relatively sharp L-edges (Bleijlevens 2002), which more closely resemble the spectra of low-spin Ni^{II} models (Van Elp *et al.* 1994; Wang *et al.* 2000; Wang *et al.* 2001a; Wang *et al.* 2001b) and of the low-spin Ni^{II} in CO-dehydrogenases from *Chlostridium thermoaceticum* and

Rhodospirillum rubrum (Ralston *et al.* 2000). For a high-spin Ni^{II} in more ionic complexes (e.g. with a predominant coordination of the Ni by O,C ligands as in the SH) even particularly pronounced splittings of the L-edge peaks are expected (Van der Laan *et al.* 1988; Wang *et al.* 2000; Wang *et al.* 2001a; Wang *et al.* 2001b), which are seemingly absent in the SH. Thus, a low-spin Ni^{II} may be present at least in the oxidized SH.

Straightforwardly, the stabilization of Ni^{II} in the SH causes the absence of Ni^{III} oxidation states. Activation of standard hydrogenases in their oxidized, inactive states containing trivalent Ni (Ni-A, Ni-B) is a slow process (minutes or longer) (Kurkin *et al.* 2004). In the SH, rapid activation occurs upon addition of NADH. Rapid activation has also been observed in the Ni-Fe-Se hydrogenase of *D. bacculatum* where the inactive Ni-A,B states are also not observable (Teixeira *et al.* 1987). Interestingly, also for this hydrogenase in its as-isolated state a low-spin Ni^{II} has been proposed (Wang *et al.* 1992). The *D. baculatum* enzyme shows elevated oxygen tolerance. The SH is not at all inhibited by oxygen. A site where the Ni^{II} oxidation state is stabilized may allow for (1) rapid activation of hydrogen-cleavage activity because the trivalent Ni-A,B states are absent, (2) oxygen tolerance, and for (3) a different mechanism of hydrogen cleavage as in the standard hydrogenases.

R. eutropha contains three Ni-Fe hydrogenases; the SH, the MBH, and the hydrogen sensor (RH). The RH detects the presence of hydrogen in the medium and triggers SH and MBH gene expression (Lenz *et al.* 2002). The rapid activation of newly synthesized SH protein may thus be a prerequisite for efficient use of H_2 as an energy source.

According to recent stopped-flow FTIR studies with the *A. vinosum* Ni-Fe hydrogenase (George *et al.* 2004; Kurkin *et al.* 2004) and earlier investigations (Roberts *et al.* 1995; DeLacey *et al.* 1997; Léger *et al.* 2002), activation of the inactive Ni-A,B states (Ni^{III}) in standard hydrogenases requires reductively induced release of an oxygen species bridging the Ni and Fe atoms (Higuchi *et al.* 1999; Carepo *et al.* 2002; Stadler *et al.* 2002; Brecht *et al.* 2003), thereby forming a catalyst, Ni-S. Both, hydrogen-cleavage and -production reaction cycles involve the same states, namely Ni-S (Ni^{II}), Ni-R (likely Ni^{II}-H^-), and Ni-C (Ni^{III}-H^-).

In the SH, the situation is clearly different. The proposed reaction sequences based on this investigation and on previous studies (Happe *et al.* 2000; Bleijlevens *et al.* 2004; Van der Linden *et al.* 2004a; Van der Linden *et al.* 2004b) are summarized in Fig. 11. Activation of the SH also involves the release of a bound oxygen species of presently unknown chemical nature. This species is likely not bound in a bridging position between Ni and Fe because this position may be blocked by the extra CN ligands. The activation process thus leads to the formation of a Ni-Fe catalyst where H_2 can be bound. If H_2 is heterolytically cleaved, formation of hydride may involve one of the remote thiolates acting as a proton acceptor and subsequent transfer of the hydride

to the FMN-a. The electrons are then forwarded via the Fe-S clusters to NAD (Van der Linden *et al.* 2004a). The 47 cm^{-1} downshift of the stretching frequency from the Ni-bound cyanide (Van der Linden *et al.* 2004b) in the SH in the presence of H$_2$ in combination with the specific feature in the XANES and the absence of shifts of the FTIR bands of CN/CO at Fe are both in agreement with binding of a H-species (H$_2$ or H$^-$) to the Ni only (Fig. 11).
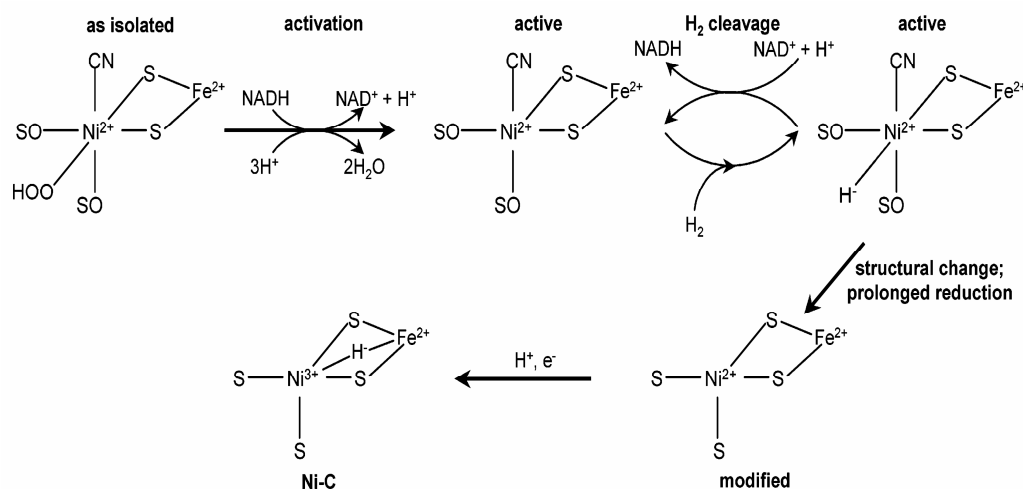

Figure 11: Tentative reaction schemes for activation and hydrogen turnover at the Ni-Fe cofactor in the SH from *R. eutropha*. The CN/CO ligands at Fe have been omitted for clarity. During activation and hydrogen cleavage, the Ni remains in the divalent oxidation state. A Ni-C state seems not to be involved. The structural changes occurring under strongly reducing conditions are proposed to lead to a standard-like Ni site. The reversibility of these changes is an open question. The modified Ni site can adopt the Ni-C state. Whether it is an intermediate during hydrogen formation requires further investigation.

A structural change of the Ni-Fe site under reducing conditions

A surprising feature of the Ni-Fe site of the SH is its susceptibility to modifications. Under prolonged reducing conditions, a modified Ni-Fe site is formed which seemingly adopts a structure similar to that of standard hydrogenases; four thiols from cysteines coordinate the Ni (Fig. 11).

In the oxidized SH, only two thiols bind the Ni; the remaining two thiols of the four conserved cysteines are more remote from the Ni. However, all four cysteines (C62, C65, C458, C461) are required for the formation of active SH (Massanz *et al.*

1999). As C62, C65, and C458 are indispensable for Ni incorporation whereas proteins mutated at C461 still bind Ni (Massanz *et al.* 1999; Burgdorf *et al.* 2002), C461 may not be a Ni ligand in the SH. The corresponding residue in *D. gigas*, Cys533, is a bridging ligand between Ni and Fe (Volbeda *et al.* 1995; Volbeda *et al.* 1996). However, the assumption that two sulphur bridges are present in the SH may lead to an overall structure of the Ni-Fe site being more similar to the one of standard hydrogenases and requiring less rearrangement of the protein matrix. Such an arrangement is, however, not uniquely implied by the available data. The remaining three cysteines are likely involved in the maturation of the Ni-Fe site (Magalon *et al.* 2000). To deduce which of the four conserved cysteines coordinates Ni in the native SH clearly requires further investigation.

Under strongly reducing conditions, seemingly oxygen species are removed from Ni. Furthermore, evidence for a conformational change resulting in the loss of the extra CN on the Ni and of FMN-a has been obtained (Axley *et al.* 1995-96; Van der Linden *et al.* 2004b) as well as for the loss of the extra CN at Fe under certain conditions (unpublished observations). Whereas FMN-a could be reincorporated, the loss of extra CN seems to be irreversible (Van der Linden *et al.* 2004b). These processes may cause open coordination sites at the Ni (and at Fe) and, during subsequent reorganizations, the more remote thiols bind Ni so that a Ni-S$_4$ site is formed. Interestingly, in the *D. desulfuricans* enzyme, the thiol group of Cys-536 (which is a terminal Ni ligand in *D. gigas* (Volbeda *et al.* 1995; Volbeda *et al.* 1996) and replaced by seleno-cysteine (Garcin *et al.* 1999) in *D. bacculatum*) has been found to be more remote from the Ni in the oxidized enzyme and to come closer to it under activating reducing conditions (Matias *et al.* 2001). Possibly, cysteine rearrangements are involved in various types of Ni-Fe hydrogenases.

In the SH, the chemically induced Ni-S$_4$ site does not seem to be able to cleave hydrogen. We have found that in certain SH preparations (here termed inactive SH), a Ni-S$_4$ site is present already after isolation under aerobic conditions, possibly due to more reducing conditions induced in the late stationary phase of heterotrophic cell growth. Hydrogen cleavage in such SH preparations was also not observed. As outlined above, the Ni-S$_4$ site may readily form the Ni-C state (Ni^{III}-H$^-$). Indeed, Ni-C was partially populated if the Ni-S$_4$ site was reductively created in the purified enzyme (Fig. 11). The bound hydride is presumably formed from a proton of the medium and electrons from the reductants. If the Ni^{III}-H$^-$ state is at all involved in hydrogen turnover by the SH, it might be an intermediate only in hydrogen production.

The effects of the point mutations

The presence of the CN at the Ni has been proposed to be related to oxygen tolerance (Happe *et al.* 2000; Bleijlevens *et al.* 2004; Van der Linden *et al.* 2004b) as the wild type SH seems to become O_2-sensitive after its specific removal (Bleijlevens *et al.* 2004; Van der Linden *et al.* 2004b). To further clarify the role of the CN ligand, two SH mutant proteins (I64A, L118F) were analyzed. Assuming homology to the structures of the crystallized standard hydrogenases (Volbeda *et al.* 1995; Volbeda *et al.* 1996; Higuchi *et al.* 1997), the respective mutations are localized at distances from the Ni of ~5 Å (I64, corresponding to V67 in the *D. gigas* structure) and ~10 Å (L118, corresponding to L115 in *D. gigas*) (Burgdorf *et al.* 2002).

In I64A, the CN ligand at the Ni seems to be replaced by an oxygen species. Ile64 connects two cysteines, C62 and C65 (Cys62-Gly63-Ile64-Cys65) (Tran-Betcke *et al.* 1990). In the *D. gigas* hydrogenase the corresponding sequence is Cys65-Gly66-Val67-Cys68 (Volbeda *et al.* 1995); C65 is one of the terminal ligands to the Ni whereas C68 provides a thiol bridge between the Ni and Fe atoms. In the SH, the replacement of I64 by alanine may thus affect the positions of C62 and C65, thereby impairing the insertion of the CN ligand. Under the tested conditions, activation of the I64A enzyme for hydrogen cleavage was impossible (Burgdorf *et al.* 2002). These results point to a function of the CN ligand in the activation process.

In L118F, XAS data analysis suggests a $(CN)_1O_2S_3$ Ni-coordination. The replacement of Leu118 by a more bulky phenylalanine may perturb the positions of three cysteines, C62, C65, and C458, thereby one of them may become an additional Ni ligand. A significant fraction of the preparation still contains the CN ligand at the Ni and activation seems to proceed as in the wild type. On the other hand, in cells containing the L118F mutant protein, SH-dependent growth is impaired at oxygen concentrations >5 % (Van der Linden *et al.* 2004b) and the hydrogen cleavage activity of the isolated enzyme is completely lost in the presence of oxygen. These results seem to imply that catalysis can become sensitive to oxygen also in the presence of the CN ligand. Oxygen sensitivity may then be caused by structural changes, e.g. binding of an additional thiol to Ni, which produce a Ni site more similar to the one of standard Ni-Fe hydrogenases.

In summary, the CN ligand at the Ni may be involved in both, establishing rapid activation and oxygen-insensitive catalytic behaviour in the SH. Possibly, one important function of the CN is stabilization of the Ni^{II} oxidation state throughout the catalytic cycle of hydrogen cleavage.

Conclusions

Analysis of the Ni-Fe cofactor of the oxygen-insensitive NAD-reducing hydrogenase (SH) from *R. eutropha* by XAS, EPR, and FTIR spectroscopy revealed a non-standard structure, $(CysS)_{0-1}(CN)(O)_3Ni^{II}(\mu\text{-}CysS)_{2-1}Fe^{II}(CN)_3(CO)$. The unusual ligation of the Ni by only two thiols plus further (C,O) ligands seems to be a prerequisite of the exceptionally rapid activation of the SH by NADH, involving the loss of an oxygen ligand from the Ni. Evidence for the binding of hydrogen to the open coordination site at Ni has been obtained. The hydrogen cleavage reaction seems not to involve a Ni-C state ($Ni^{III}\text{-}H^-$). Prolonged reducing conditions cause a structural change, which converts the native Ni-Fe site to a $Ni(CysS)_4$ site, similar to that found in standard hydrogenases. The $Ni(CysS)_4$ site can form the Ni-C state also in the SH. Comparison of two mutants and wild type enzyme points to a role of the extra CN ligand at the Ni in stabilization of the Ni^{II} oxidation state and in the activation process besides of a function in establishing oxygen-insensitive catalysis.

References

Albracht, S. P. J. (1994). ″Nickel hydrogenases: in search of the active site″ *Biochim. Biophys. Acta* **1188**: 167-204.

Albracht, S. P. J. and Hedderich, R. (2000). ″Learning from hydrogenases: location of a proton pump and of a second FMN in bovine NADH--ubiquinone oxidoreductase (Complex I)″ *FEBS Letters* **485** (1): 1-6.

Albracht, S. P. J., Van der Linden, E. and Faber, B. W. (2003). ″Quantitative amino acid analysis of bovine NADH:ubiquinone oxidoreductase (Complex I) and related enzymes. Consequences for the number of prosthetic groups″ *Biochim. Biophys. Acta* **1557** (1-3): 41-49.

Amara, P., Volbeda, A., Fontecilla-Camps, J. C. and Field, M. J. (1999). ″A Hybrid Density Functional Theory/Molecular Mechanics Study of Nickel-Iron Hydrogenase: Investigation of the Active Site Redox States″ *J. Am. Chem. Soc.* **121**: 4468-4477.

Ankudinov, A. L., Ravel, B., Rehr, J. J. and Conradson, S. D. (1998). ″Real-space multiple-scattering calculation and interpretation of x-ray-absorption fine structure″ *Phys. Rev. B* **12**: 7565-7576.

Axley, M. J., Keefe, R. G., Falk, M. C. and Harabin, A. L. (1995-96). ″FMN cofactor dissociation from the soluble hydrogenase of *Alcaligenes eutrophus* H16″ *Biofactors* **5** (2): 87-92.

Bagley, K. A., Duin, E. C., Roseboom, W., Albracht, S. P. J. and Woodruff, W. H. (1995). ″Infrared-Detectable Groups Sense Changes in Charge Density on the Nickel Center in Hydrogenase from *Chromatium vinosum*″ *Biochemistry* **34**: 5527-5535.

Bagley, K. A., Van Garderen, C. J., Chen, M., Duin, E. C., Albracht, S. P. J. and Woodruff, W. H. (1994). ″Infrared studies on the interaction of carbon monoxide with divalent nickel in hydrogenase from *Chromatium vinosum*″ *Biochemistry* **33** (31): 9229-9236.

Benfatto, M., Della Longa, S. and Natoli, C. R. (2003). ″The MXAN procedure: a new method for analysing the XANES spectra of metalloproteins to obtain structural quantitative information″ *J. Synchrotron Rad.* **10**: 51-57.

Berkessel, A. (2001). ″Activation of dihydrogen without transition metals.″ *Curr. Opin. Chem. Biol.* **5** (5): 486-490.

Bernhard, M., Buhrke, T., Bleijlevens, B., DeLacey, A. L., Fernandez, V. M., Albracht, S. P. J. and Friedrich, B. (2001). ″The H_2 Sensor of *Ralstonia eutropha*″ *J. Biol. Chem.* **276** (19): 15592-15597.

Bernhard, M., Schwartz, E., Rietdorf, J. and Friedrich, B. (1996). "The *Alcaligenes eutrophus* Membrane-Bound Hydrogenase Gene Locus Functions Involved in Maturation and Electron Transport Coupling" *J. Bacteriol.* **178** (15): 4522-4529.

Bleijlevens, B. (2002). Ph. D. Thesis, University of Amsterdam

Bleijlevens, B., Buhrke, T., Van der Linden, E., Friedrich, B. and Albracht, S. P. J. (2004). "The auxiliary protein HypX provides oxygen tolerance to the soluble [NiFe]-hydrogenase of *Ralstonia eutropha* H16 by way of a cyanide ligand to nickel" *J. Biol. Chem.* **in press**.

Bradford, M. (1976). "A Rapid and Sensitive Method for the Quantitation of Microgram Quantities of Protein Utilizing the Principle of Protein-Dye Binding" *Analytical Biochemistry* **72**: 248 - 254.

Brecht, M., Van Gastel, M., Buhrke, T., Friedrich, B. and Lubitz, W. (2003). "Direct Detection of a Hydrogen Ligand in the [NiFe] Center of the Regulatory H_2-Sensing Hydrogenase from *Ralstonia eutropha* in Its Reduced State by HYSCORE and ENDOR Spectroscopy" *J. Am. Chem. Soc.* **125**: 13075 - 13083.

Burgdorf, T., DeLacey, A. L. and Friedrich, B. (2002). "Functional Analysis by Site-Directed Mutagenesis of the NAD^+-Reducing Hydrogenase from *Ralstonia eutropha*" *Journal of Bacteriology* **184** (22): 6280-6288.

Cammack, R., Robson, R. and Frey, M. (1997). Hydrogen as a fuel: Learning from nature. London, UK, Taylor & Francis.

Carepo, M., Tierney, D. L., Brondino, C. D., Yang, T. C., Pamplona, A., Telser, J., Moura, I., Moura, J. J. and Hoffman, B. M. (2002). "^{17}O ENDOR Detection of a Solvent-Derived Ni-(OH$_x$)-Fe Bridge That Is Lost upon Activation of the Hydrogenase from *Desulfovibrio gigas*" *J. Am. Chem. Soc.* **124** (2): 281-286.

Colpas, G. J., Maroney, M. J., Bagyinka, C., Kumar, M., Willis, W. S., Suib, S. L., Mascharak, P. K. and Baidya, N. (1991). "X-ray spectroscopic studies of nickel complexes, with application to the structure of nickel sites in hydrogenases" *Inorg. Chem.* **30** (5): 920-928.

Coremans, J. M., Van der Zwaan, J. W. and Albracht, S. P. J. (1992a). "Distinct redox behaviour of prosthetic groups in ready and unready hydrogenase from *Chromatium vinosum*." *Biochim. Biophys. Acta* **26** (119): 2.

Coremans, J. M., Van Garderen, C. J. and Albracht, S. P. J. (1992b). "On the redox equilibrium between H2 and hydrogenase" *Biochim. Biophys. Acta* **1119** (2): 148-56.

Dau, H., Liebisch, P. and Haumann, M. (2003). "X-ray absorption spectroscopy to analyze nuclear geometry and electronic structure of biological metal centers-potential and questions examined with special focus on the tetra-nuclear

manganese complex of oxygenic photosynthesis" *Analyt. Bioanalyt. Chem.* **376** (5): 562 - 583.

Davidson, G., Choudhury, S. B., Gu, Z., Bose, K., Roseboom, W., Albracht, S. P. J. and Maroney, M. J. (2000). "Structural Examination of the Nickel Site in *Chromatium vinosum* Hydrogenase: Redox State Oscillations and Structural Changes Accompanying Reduktive Activation and CO Binding" *Biochemistry* **39**: 7468-7479.

Davis, D. H., Doudoroff, M., Stanier, R. Y. and Mandel, M. (1969). *Int. J. Syst. Bacteriol.* **19**: 375-390.

DeLacey, A. L., Hatchikian, E. C., Volbeda, A., Frey, M., Fontecilla-Camps, J. C. and Fernandez, V. M. (1997). "Infrared-Spectroelectrochemical Characterization of the [NiFe] Hydrogenase of *Desulfovibrio gigas*" *J. Am. Chem. Soc.* **119**: 7181-7189.

Dittmer, J. (1999). *Linear-Dichroismus-Röntgenabsorptionsspektroskopie zum katalytischen Zyklus des wasserspaltenden Mangan-Komplexes der Photosynthese in Theorie und Experiment*, Ph. D. Thesis, Christian Albrechts-Universität

Eidsness, M. K., Sullivan, R. J. and Scott, R. J. (1988). Electronic molecular structure of biological Nickel as studied by X-ray absorption spectroscopy. The bioanorganic chemistry of nickel. J. R. Lancaster. New York, USA, VCH Publisher.

Erkens, A., Schneider, K. and Müller, A. (1996). "The NAD-linked soluble hydrogenase from *Alcaligenes eutrophus* H16: detection and characterization of EPR signals deriving from nickel and flavin" *J. Biol. Inorg. Chem.* **1**: 99-110.

Fan, C., Teixeira, M., Moura, J. J. G., Moura, I., Huynh, B. H., Legall, J., Peck, H. D. J. and Hoffman, B. M. (1991). "Detection and Characterization of Exchangeable Protons Bound to the Hydrogen-Activaton Nickel Site of *Desulfovibrio gigas* Hydrogenase: A ^{1}H and ^{2}H Q-Band ENDOR study" *J. Am. Chem. Soc.* **113**: 20-24.

Fan, H.-J. and Hall, M. B. (2002). "High-Spin Ni(II), a Surprisingly Good Structural Model for [NiFe] Hydrogenase" *J. Am. Chem. Soc.* **124** (3): 394-395.

Foerster, S., Stein, M., Brecht, M., Ogata, H., Higuchi, Y. and Lubitz, W. (2003). "Single Crystal EPR Studies of the Reduced Active Site of [NiFe] Hydrogenase from *Desulfovibrio vulgaris* Miyazaki F" *J. Am. Chem. Soc.* **125**: 83-93.

Fontecilla-Camps, J. C., Frey, M., Garcin, E., Hatchikian, C., Montet, Y., Piras, C., Vernede, X. and Volbeda, A. (1997). "Hydrogenase: a hydrogen-metabolizing enzyme. What do the crystal structures tell us about its mode of action?" *Biochimie* **79** (11): 661-666.

Fox, S., Wang, Y., Silver, A. and Millar, M. (1990). "Viability of the [Ni^{III}(SR)$_4$] -Unit in Classical Coordination Compounds and in the Nickel-Sulfur Center of Hydrogenases" *J. Am. Chem. Soc.* **112**: 3218-3220.

Frey, M. (2002). "Hydrogenases: Hydrogen-Activating Enzymes" *Chem. Biochem.* **3**: 153-160.

Friedrich, B., Heine, E., Finck, A. and Friedrich, C. G. (1981). "Nickel requirement for active hydrogenase formation in Alcaligenes eutrophus" *J. Bacteriol.* **145** (3): 1144-1149.

Friedrich, B. and Schwartz, E. (1993). "Molecular Biology of Hydrogen Utilization in Aerobic Chemolithotrophs" *Ann. Rev. Microbiol.* **47**: 351-383.

Friedrich, C. G., Schneider, K. and Friedrich, B. (1982). "Nickel in the catalytically active hydrogenase of Alcaligenes eutrophus" *J. Bacteriol.* **152** (1): 42-48.

Garcin, E., Vernède, X., Hatchikian, E. C., Volbeda, A., Frey, M. and Fontecilla-Camps, J. C. (1999). "The crystal structure of a reduced [NiFeSe] hydrogenase provides an image of the activated catalytic center" *Structure Fold. Des.* **7** (5): 557-566.

George, S. J., Kurkin, S., Thorneley, R. N. F. and Albracht, S. P. J. (2004). "Reactions of H2, CO, and O2 with Active [NiFe]-Hydrogenase from *Allochromatium vinosum*. A Stopped-Flow Infrared Study" *Biochemistry* **43** (21): 6808 - 6819.

Gu, W., Jacquamet, L., Patil, D. S., Wang, H.-X., Evans, D. J., Smith, M. C., Millar, M., Koch, S., Eichhorn, D. M., Latimer, M. and Cramer, S. P. (2003). "Refinement of the nickel site structure in *Desulfovibrio gigas* hydrogenase using range-extended EXAFS spectroscopy" *Journal of Inorganic Biochemistry* **93**: 41-51.

Gu, Z., Dong, J., Allan, C. B., Choudhury, S. B., Franco, R., Moura, J. J. G., Moura, I., Legall, J., Przybyla, A. E., Roseboom, W., Albracht, S. P. J., Axley, M. J., Scott, R. A. and Maroney, M. J. (1996). "Structure of the Ni Sites in Hydrogenases by X-ray Absorption Spectroscopy. Species Variation and the Effects of Redox Poise" *J. Am. Chem. Soc.* **118**: 11155-11165.

Haines, R. I. and McAuley, A. (1981). "Synthesis and reactions of nickel(III) complexes." *Coordination Chem. Rev.* **39** (1-2): 77-119.

Happe, R. P., Roseboom, W., Egert, G., Friedrich, C. G., Massanz, C., Friedrich, B. and Albracht, S. P. J. (2000). "Unusual FTIR and EPR properties of the H$_2$-activatiing site of the cytoplasmic NAD-reducing hydrogenase from *Ralstonia eutropha*" *FEBS Letters* **466**: 259-263.

Happe, R. P., Roseboom, W., Pierik, A. J., Albracht, S. P. J. and Bagley, K. A. (1997). "Biological activation of hydrogen" *Nature* **385** (6612): 126.

Haumann, M., Porthun, A., Buhrke, T., Liebisch, P., Meyer-Klaucke, W., Friedrich, B. and Dau, H. (2003). "Hydrogen-Induced Structural Changes at the Nickel Site of the Regulatory [NiFe] Hydrogenase from *Ralstonia eutropha* Detected by X-ray Absorption Spectroscopy." *Biochemistry* **42** (37): 11004-15.

Higuchi, Y., Ogata, H., Miki, K., Yasuoka, N. and Yagi, T. (1999). "Removal of the bridging ligand atom at the Ni-Fe active site of [NiFe] hydrogenase upon reduction with H2, as revealed by X-ray structure analysis at 1.4 A resolution" *Structure Fold. Des.* **7** (5): 549-56.

Higuchi, Y., Yagi, T. and Yasuoka, N. (1997). "Unusual ligand structure in Ni-Fe active center and an additional Mg site in hydrogenase revealed by high resolution X-ray structure analysis" *Structure* **5** (12): 1671-1680.

Horner, D. S., Heil, B., Happe, T. and Embley, T. M. (2002). "Iron hydrogenases – ancient enzymes in modern eukaryotes" *Trends Biochem. Sci.* **7** (3): 148-153.

Iuzzolino, L., Dittmer, J., Dörner, W., Meyer-Klaucke, W. and Dau, H. (1998). "X-ray Absorption Spectroscopy on Layered Photosystem II Membrane Particles Suggests Manganese-Centered Oxidation of the Oxygen-Evolving Complex for the S0-S1, S1-S2, and S2-S3 Transitions of the Water Oxidation Cycle" *Biochemistry* **37**: 17112 - 17119.

Keefe, R. G., Axley, M. J. and Harabin, A. L. (1995). "Kinetic Mechanism Studies of the Soluble Hydrogenase from *Alcaligenes eutrophus* H16" *Archives Biochem. Biophys.* **317** (2): 449-456.

Kleihues, L., Lenz, O., Bernhard, M., Buhrke, T. and Friedrich, B. (2000). "The H_2 Sensor of *Ralstonia eutropha* Is a Member of the Subclass of Regulatory [NiFe] Hydrogenases" *J. Bacteriol.* **182** (10): 2716-2724.

Koningsberger, D. C., Mojet, B. L., Van Dorssen, G. E. and Ramaker, D. E. (2000). "XAFS spectroscopy; fundamental principles and data analysis" *Topics in Catalysis* **10**: 143-155.

Kurkin, S., George, S. J., Thorneley, R. N. F. and Albracht, S. P. J. (2004). "Hydrogen-Induced Activation of the [NiFe]-Hydrogenase from *Allochromatium vinosum* as Studied by Stopped-Flow Infrared Spectroscopy" *Biochemistry* **43** (21): 6820 - 6831.

Léger, C., Jones, A. K., Roseboom, W., Albracht, S. P. J. and Armstrong, F. A. (2002). "Enzyme Electrokinetics: Hydrogen Evolution and Oxidation by *Allochromatium vinosum* [NiFe]-Hydrogenase" *Biochemistry* **41**: 15736-15746.

Lenz, O., Bernhard, M., Buhrke, T., Schwartz, E. and Friedrich, B. (2002). "The Hydrogen-Sensing Apparatus in *Ralstonia eutropha*" *J. Mol. Microbiol. Biotech.* **4** (3): 255-262.

Lenz, O. and Friedrich, B. (2001). ″Bakterielle Wasserstoff-Sensoren" *Biospektrum* **6**: 515-520.

Lubitz, W., Brecht, M., Foerster, S., Stein, M., Higuchi, Y., Buhrke, T. and Friedrich, B. (2002). EPR and theoretical investigations of [NiFe] hydrogenase: Insight into the mechanism of biological hydrogen conversion. Amsterdam, Netherland, Elsevier.

Magalon, A. and Bock, A. (2000). ″Analysis of the HypC-hycE complex, a key intermediate in the assembly of the metal center of the Escherichia coli hydrogenase 3" *J. Biol. Chem.* **275** (28): 21114-20.

Maroney, M. J. (1999). ″Structure/ function relationships in nickel metallobiochemistry" *Curr. Opin. in Chem. Biol.* **3**: 188-199.

Massanz, C. and Friedrich, B. (1999). ″Amino Acid Replacements at the H_2-Activating Site of the NAD-Reducing Hydrogenase from *Alcaligenes eutrophus*" *Biochemistry* **38** (43): 14330-14337.

Massanz, C., Schmidt, S. and Friedrich, B. (1998). ″Subforms and In Vitro Reconstitution of the NAD-Reducing Hydrogenase of *Alcaligenes eutrophus*" *J. Bacteriol.* **180** (5): 1023-1029.

Matias, P. M., Soares, C. M., Saraiva, L. M., Coelho, R., Morais, J., Legall, J. and Carrondo, M. A. (2001). ″[NiFe] hydrogenase from Desulfovibrio desulfuricans ATCC 27774: gene sequencing, three-dimensional structure determination and refinement at 1.8 A and modelling studies of its interaction with the tetrahaem cytochrome c3" *J. Biol. Inorg. Chem.* **6** (1): 63-81.

Mayhew, S. G. (1978). ″The redox potential of dithionite and SO-2 from equilibrium reactions with flavodoxins, methyl viologen and hydrogen plus hydrogenase" *Eur. J. Biochem.* **85** (2): 535-547.

Meinke, C., Sole, V. A., Pospisil, P. and Dau, H. (2000). ″Does the structure of the water-oxidizing photosystem II-manganese complex at room temperature differ from its low-temperature structure? A comparative X-ray absorption study" *Biochemistry* **39** (24): 7033-7040.

Mijovilovich, A. and Meyer-Klaucke, W. (2003). ″Simulating the XANES of metalloenzymes - a case study
A. Mijovilovich and W. Meyer-Klaucke" *J. Synchrotron Rad.* **10**: 64-68.

Müller, A., Erkens, A., Müller, A., Schneider, K., Nolting, H.-F., Solé, V. A. and Henkel, G. (1997). ″NADH-induzierte Einflüsse auf die Koordination des Nickels im aktiven Zentrum der löslichen Hydrogenase aus *Alcaligenes eutrophus*: XAFS-Untersuchungen an drei ESR-spektroskopisch unterscheidbaren Zuständen" *Angew. Chem.* **106** (16): 1812-1815.

Müller, A., Tscherny, I., Kappl, R., Hatchikian, E. C., Hüttermann, J. and Cammack, R. (2002). "Hydrogenases in the "active" state: determination of *g*-matrix axes and electron spin distribution at the active site by ^{1}H ENDOR spectroscpoy" *J. Biol. Inorg. Chem.* **7**: 177-194.

Nag, K. C., A. (1980). "Monovalent, trivalent and tetravalent nickel" *Coordination Chem. Rev.* **33** (2): 87-147.

Nicolet, Y., Piras, C., Leger, P., Hatchikian, C. E. and Fontecilla-Camps, J. C. (1999). "Desulfovibrio desulfuricans iron hydrogenase: the structure shows unusual coordination to an active site Fe binuclear center." *Struc. Fold. Des.* **7** (1): 13-23.

Niu, S., Thomsom, L. M. and Hall, M. B. (1999). "Theoretical Characterization of the Reaction Intermediates in a Model of the Nickel-Iron Hydrogenase of *Desulfovibrio gigas*" *J. Am. Chem. Soc.* **121**: 4000-4007.

Peters, J. W., Lanzilotta, W. N., Lemon, B. J. and Seefeldt, L. C. (1998). "X-ray Crystal Structure of the Fe-Only Hydrogenase (Cpl) from *Clostridium pasteurianum* to 1.8 Angstrom Resolution" *Science* **282**: 1853-1858.

Pettifer, R. F. and Hermes, C. (1985). "Absolute energy calibration of x-ray radiation from synchrotron sources" *J. Appl. Crystall.* **18** (6): 404-12.

Pierik, A. J., Roseboom, W., Happe, R. P., Bagley, K. A. and Albracht, S. P. J. (1999). "Carbon Monoxide and Cyanide as Intrinsic Ligands to Iron in the Active Site of [NiFe]-Hydrogenases" *J. Biol. Chem.* **274** (6): 3331-3337.

Pilkington, S. J., Skehel, J. M., Gennis, R. B. and Walker, J. E. (1991). "Relationship between mitochondrial NADH-ubiquinone reductase and a bacterial NAD-reducing hydrogenase" *Biochemistry* **30** (8): 2166-2175.

Przybyla, A. E., Robbins, J., Menon, N. and Peck, H. D. J. (1992). "Structure-function relationships among the nickel-containing hydrogenases" *FEMS Microbiol. Rev.* **8** (2): 109-135.

Ralston, C. Y., Wang, H., Ragsdale, S. W., Kumar, M., Spangler, N. J., Ludden, P. W., Gu, W., Jones, R. M., Patil, D. S. and Cramer, S. P. (2000). "Characterization of Heterogeneous Nickel Sites in CO Dehydrogenases from *Clostridium thermoaceticum* and *Rhodospirillum rubrum* by Nickel L-Edge X-ray Spectroscpoy" *J. Am. Chem. Soc.* **122**: 10553-10560.

Rehr, J. J. and Ankudinov, A. L. (2001). "Progess and challenges in the theory and interpretation of X-ray spectra" *J. Synchrotron Rad.* **8**: 61-65.

Reissmann, S., Hochleitner, E., Wang, H., Paschos, A., Lottspeich, F., Glass, R. S. and Böck, A. (2003). "Taming of a Poison: Biosynthesis of the NiFe-Hydrogenase Cyanide Ligands" *Science* **299**: 1067-1070.

Roberts, L. M. and Lindahl, P. A. (1995). "Stoichiometric Reductive Titrations of *Desulfovibrio gigas* Hydrogenase" *J. Am. Chem. Soc.* **117**: 2565-2572.

Schiller, H., Dittmer, J., Iuzzolino, l., Dörner, W., Meyer-Klaucke, W., Solé, V. A., Nolting, H.-F. and Dau, H. (1998). "Structure and Orientation of the Oxygen-Evolving Manganese Complex of Green Algae and Higher Plants Investigated by X-ray Absorption Linear Dichroism Spectroscopy on Oriented Photosystem II Membrane Particles" *Biochemistry* **37**: 7340 - 7350.

Schink, B. S., H. G. (1979). "The membrane-bound hydrogenase of *Alcaligenes eutrophus*. I. Solubilization, purification, and biochemical properties" *Biochim. Biophys. Acta* **567** (2): 315-324.

Schneider, K., Cammack, R., Schlegel, H. G. and Hall, D. O. (1979). "The Iron-Sulphur Centres of Soluble Hydrogenase from *Alcaligenes eutrophus*" *Biochim. Biophys. Acta* **578**: 445-461.

Schneider, K., Erkens, A. and Müller, A. (1996). "On the Structure and Function of the Active Center of the NAD-Linked Hydrogenase from *Alcaligenes eutrophus* H16" *Naturwissenschaften* **83**: 78-81.

Schneider, K. and Schlegel, H. G. (1976). "Purification and properties of soluble hydrogenase from *Alcaligenes eutrophus* H 16" *Biochim. Biophys. Acta* **452**: 66-80.

Scott, R. A. (2000). Physical Methods in Bioinorganic Chemistry. Sausalito, USA, University Science Books.

Siegbahn, P. E. M., Blomberg, M. R. A., Wirstam nee Pavlov, M. and Crabtree, R. H. (2001). "The mechanism of the Ni-Fe hydrogenases: a quantum chemical perspective." *J. Biol. Inorg. Chem.* **6** (4): 460-466.

Stadler, C., DeLacey, A. L., Montet, Y., Volbeda, A., Fontecilla-Camps, J. C., Conesa, J. C. and Fernandez, V. M. (2002). "Density Functional Calculations for Modeling the Active Site of Nickel-Iron Hydrogenases. 2. Predictions for the Unready and Ready States and the Corresponding Activation Processes" *Inorg. Chem.* **41**: 4424-4434.

Stein, M. and Lubitz, W. (2002). "Quantum chemical calculations of [NiFe] hydrogenase" *Curr. Opin. Chem. Biol.* **6**: 243-249.

Stöhr, J. (1992). NEXAFS Spectroscopy. Berlin, Germany, Springer Verlag.

Teixeira, M., Fauque, G., Moura, I., Lespinat, P. A., Berlier, Y., Prickril, B., Peck, H. D. J., Xavier, A. V., Le Gall, J. and Moura, J. J. (1987). "Nickel-[iron-sulfur]-selenium-containing hydrogenases from Desulfovibrio baculatus (DSM 1743). Redox centers and catalytic properties" *Eur. J. Biochem.* **167** (1): 47-58.

Teo, B. (1986). EXAFS: Basic Principles and Data Analysis. Berlin, Germany, Springer Verlag.

Tran-Betcke, A., Warnecke, U., Böcker, C., Zaborosch, C. and Friedrich, B. (1990). ″Cloning and nucleotide sequences of the genes for the subunits of NAD-reducing hydrogenase of *Alcaligenes eutrophus* H16.″ *J. Bacteriol.* **172** (6): 2920-2929.

Trofanchuk, O., Stein, M., Geßner, C., Lendzian, F., Higuchi, Y. and Lubitz, W. (2000). ″Single crystal EPR studies of the oxidized active site of [NiFe] hydrogenase from *Desulfovibrio vulgaris* Miyazaki F″ *J. Biol. Inorg. Chem.* **5**: 36-44.

Van der Laan, G., Thole, B. T. and Sawatzky, G. A. (1988). ″Multiplet structure in the L2,3 x-ray-absorption spectra: A fingerprint for high- and low-spin Ni2+ compounds″ *Phys. Rev. B* **37**: 6587–6589.

Van der Linden, E., Bart, W., Faber, B., Bleijlevens, B., Burgdorf, T., Bernhard, M., Friedrich, B. and Albracht, S. P. J. (2004a). ″Selective release and function of one of the two FMN groups in the cytoplasmic NAD+-reducing [NiFe]-hydrogenase from *Ralstonia eutropha*″ *Eur. J. Biochem.* **271**: 801-808.

Van der Linden, E., Burgdorf, T., Bernhard, M., Bleijlevens, B., Friedrich, B. and Albracht, S. P. J. (2004b). ″The soluble [NiFe]-hydrogenase from *Ralstonia eutropha* contains four cyanides in its active site, one of which is responsible for the insensitivity towards oxygen″ *J. Biol. Inorg. Chem.* **9**: 616-626.

Van der Zwaan, J. W., Albracht, S. P. J., Fontijn, R. D. and Mul, P. (1987). ″On the anomalous temperature behaviour of the EPR signal of monovalent nickel in hydrogenase″ *Eur. J. Biochem.* **169** (2): 377-84.

Van der Zwaan, J. W., Albracht, S. P. J., Fontijn, R. D. and Slater, E. C. (1985). ″Monovalent nickel in hydrogenase from *Chromatium vinosum.* Light sensitivity and evidence for direct interaction with hydrogen.″ *FEBS Letters* **179** (2): 271-277.

Van Elp, J., Peng, G., Searle, B. G., Mitra-Kirtley, S., Huang, Y. H., Johnson, M. K., Zhou, Z. H., Adams, M. W., Maroney, M. J. and Cramer, S. P. (1994). ″Electronic Structure and Symmetry in Nickel L Edge X-ray Absorption Spectroscopy: Application to a Nickel Protein″ *J. Am. Chem. Soc.* **116** (5): 1918-23.

Vanechoutte, M., Kampfer, P., De Baere, T., Falsen, E. and Verschraegen, G. (2004). *Int. J. Syst. Evol. Microbiol.* **54**: 317-327.

Vignais, P. M., Billoud, B. and Meyer, J. (2001). ″Classification and phylogeny of hydrogenases″ *FEMS Microbiol. Rev.* **25** (4): 455-501.

Volbeda, A., Charon, M. H., Piras, C., Hatchikian, E. C., Frey, M. and Fontecilla-Camps, J. C. (1995). ″Crystal structure of the nickel-iron hydrogenase from *Desulfovibrio gigas*″ *Nature* **373** (6515): 556-557.

Volbeda, A., Garcin, E., Piras, C., De Lacey, A. L., Fernandez, V. M., Hatchikian, E. C., Frey, M. and Fontecilla-Camps, J. C. (1996). ″Structure of the [NiFe] Hydrogenase Active Site: Evidence for Biologically Uncommon Fe Ligands″ *J. Am. Chem. Soc.* **118** (51): 12989 - 12996.

Wang, C. P., Franco, R., Moura, J. J., Moura, I. and Day, E. P. (1992). ″The nickel site in active Desulfovibrio baculatus [NiFeSe] hydrogenase is diamagnetic. Multifield saturation magnetization measurement of the spin state of Ni(II)″ *J. Biol. Chem.* **267** (11): 7378-80.

Wang, H., Patil, D. S., Gu, W., Jacquamet, L., Friedrich, S., Funk, T. and Cramer, S. P. (2001a). ″L-edge X-ray absorption spectroscopy of some Ni enzymes: probe of Ni electronic structure″ *J. Electron Spectrosc.. Relat. Phenomen.* **114-116**: 855-863.

Wang, H., Patil, D. S., Ralston, C. Y., Bryant, C. and Cramer, S. P. (2001b). ″L-Edge X-ray magnetic circular dichroism of Ni enzymes: direct probe of Ni spin states″ *J. Electron Spectrosc.. Relat. Phenomen.* **114-116**: 865-871.

Wang, H., Ralston, C. Y., Patil, D. S., Jones, R. M., Gu, W., Verhagen, M., Adams, M., Ge, P., Riordan, C., Marganian, C. A., Mascharak, P. K., Kovacs, J., Miller, C. G., Collins, C. J., Brooker, S., Croucher, P. D., Wang, K., Stiefel, E. I. and Cramer, S. P. (2000). ″Nickel L-Edge Soft X-ray Spectroscopy of Nickel - Iron Hydrogenases and Model Compounds - Evidence for High-Spin Nickel(II) in the Active Enzyme″ *J. Am. Chem. Soc.* **122**: 10544-10552.

Wilde, E. (1962). *Arch. Microbiol.* **43**: 157-185.

Yabuuchi, E., Kosako, Y., Yano, I., Hotta, H. and Nishiuchi, Y. (1995). *Microbiol. Immunol* **19**: 897-904.

Zabinsky, S. I., Rehr, J. J., Aukudinov, A., Albers, R. C. and Eller, M. J. (1995). ″Multiple-scattering calculations of x-ray-absorption spectra″ *Phys. Rev. B* **52** (4): 2995-3009.